Modelling wind turbine wakes for wind farms

Modelling wind turbine wakes for wind farms

Angus C. W. Creech[1]. Institute of Energy Systems, University of Edinburgh, Edinburgh EH9 3JL, Scotland
Wolf-Gerrit Früh[2]. School of Engineering and Physical Sciences, Heriot-Watt University, Edinburgh EH14 4AS, Scotland

1 Abstract

The simulation of the wakes behind wind turbines is important in predicting energy yields in wind farms, and so plays a role in planning the layout of these farms. As both wind turbines and farms increase in size, wind farm modellers have faced challenges as previously-held assumptions and parameterisations become inadequate – requiring more detailed, less parameterised methods such as those available through computational fluid dynamics. In this article the authors chart the progress of wind turbine wake modelling from analytical methods towards computational fluid dynamics, discussing approaches such as Reynolds-averaged Navier-Stokes and Large Eddy Simulation.

2 Introduction

This section sets the scene for the importance of wake modelling by first placing it in the context of the other wind farm design tasks, observations of the effect of a wind turbine's wake on other turbines in a farm and the consequence on the overall performance of the wind farm. To conclude this section we will return to the behaviour of an isolated turbine wake, to illustrate the main processes affecting turbine wakes which need to be adequately covered by wake models.

2.1 Wind farm design

Designing a large wind farm involves a number of tasks, including estimating the available wind resource from local and regional data, environmental assessments – such as visual intrusion, noise and impacts on wild life – the local wind distribution at the proposed locations of the turbine, and many more. It is therefore important to provide tools for these tasks which are at the same time accurate, reliable, and cost-effective. With the development in computing power, it is now common practice to carry out flow modelling of the air flow through the proposed wind farm, and there are a number of commercial products and services to provide this.

However a full flow model including just the most important factors would require representation of the topography at a fairly high resolution, allow for small-scale convection through heat fluxes from the surface, turbulence generation, transport and decay, as well the effect of the wind on wind turbines and vice versa. All these processes would then have to be applied to a variety of meteorological conditions in terms of wind speeds, wind direction and atmospheric stability as is needed to obtain a fair representation of the chosen wind farm site. Furthermore, in the design stage these modelling activities only become really useful if they can be used to optimise the layout of the turbines, which implies repeating all the meteorological conditions for a range of turbine locations.

Considering this range of demands, it is immediately obvious that such a task is only possible by representing many of these processes through highly simplified parameterisations. For example, the major effect of heat fluxes on the flow structures relevant to large turbine rotors is the vertical shear. Instead of modelling the actual heat fluxes and resulting buoyancy forces in the models, they are

[1] Email: a.c.w.creech@hw.ac.uk
[2] Email: w.g.fruh@hw.ac.uk

frequently only represented by imposing a typical wind shear profile as boundary conditions. The aerodynamics of the turbine blades would in direct simulations require a full description of the rotating solid blades with boundary conditions requiring a very high resolution; these are usually replaced by a body force determined from the performance of the rotor in the form of what is known as an Actuator Disk, or through the lift and drag coefficients from Boundary Element Momentum theory, or similar approaches. Similarly, the wake behind a turbine and its gradual decay is usually represented through a much simplified empirical or semi-empirical parameterisation.

2.2 Observed wake effects

As wind farms become progressively larger, where many new projects have hundreds of MW-rated turbines, it is becoming very important to know what effect a turbine has on other turbines in the farm and what the combined effect of a large wind farm could be on the environment. These effects could be on electrical, for example on power quality issues from connecting the farm to the grid. On the aerodynamic side, a wind turbine affects the flow and causes in a wake downstream of the turbine rotor in which the mean velocity is decreased, a rotation of the air induced, and substantial turbulence generated: another turbine placed in such a wake will experience very different air flow conditions than an isolated turbine. The consequences are that a downstream turbine may produce less power due to the reduced mean flow and that turbine blades may experience stronger fluctuations in their loadings and stresses due to the induced turbulence.

From the perspective of a wind farm developer, it is important to maximise the net income from electricity production from a given available area. Hence, it is important to optimise the spacing of turbines to install as many as possible while spacing them with sufficient distance to limit the wake effects.

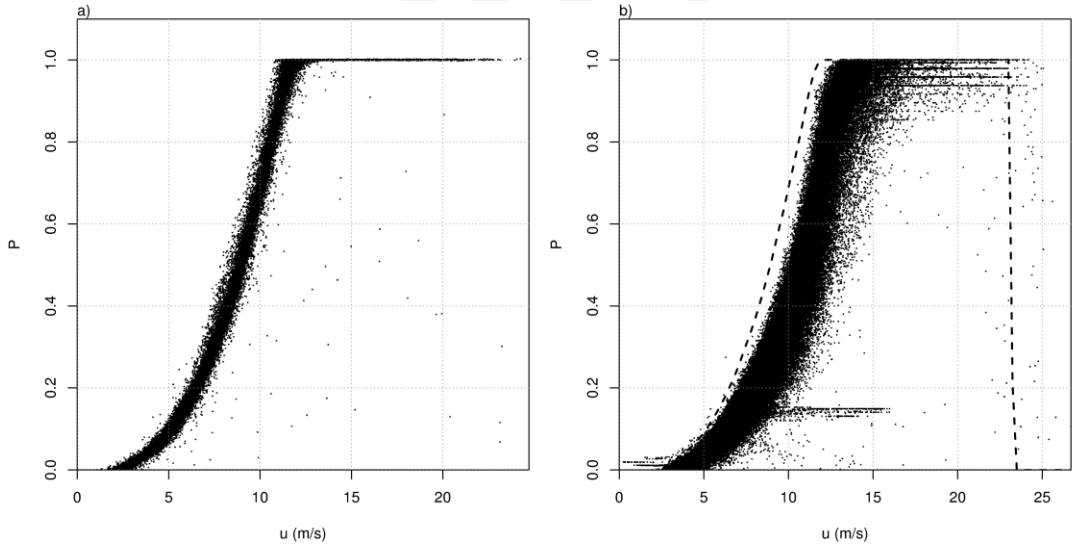

Figure 1. Turbine and farm performance curves. Data source: Vattenfall.

It is best to illustrate the magnitude from results of the Lillgrund offshore wind farm which consists of a relatively regular array of 48 fairly closely spaced turbines [31]. Figure 1 compares the power curve for one of the turbines of that wind farm with the power curve for the entire wind farm, the former scaled against the rated power of the turbine, the latter against the installed capacity of the wind farm. Figure 1.a) shows the power output for one of the turbines in the front row relative to the prevailing wind direction, where only the cases were included when the wind came from a 120º sector surrounding that direction. The wind speed is that measured from the nacelle anemometer and the power output shows clearly the cut-in wind speed, the increase to the rated power, and the range where the turbine operates at the rated power, and the scatter is relatively tight. Contrasted

with this, Figure 1.b) shows the total wind farm output against nacelle wind speed of the most exposed wind for all wind directions. The wind farm perform not only shows a much larger scatter but the entire performance curve is shifted to the right, to higher wind speeds. To better show the shift of the performance curve, the averaged performance from the individual turbine in Figure 1.a) is superimposed as the dashed line. The additional horizontal lines correspond to individual turbines being switched off rather than external wind conditions. However, the consistent shift of the curve to higher wind speeds can only be explained by shading of turbines situated in the wake of upstream turbines, and the much larger scatter can be explained by the fact that it depended very much on the wind direction as to how much turbines in the second and further rows are affected by upstream wakes.

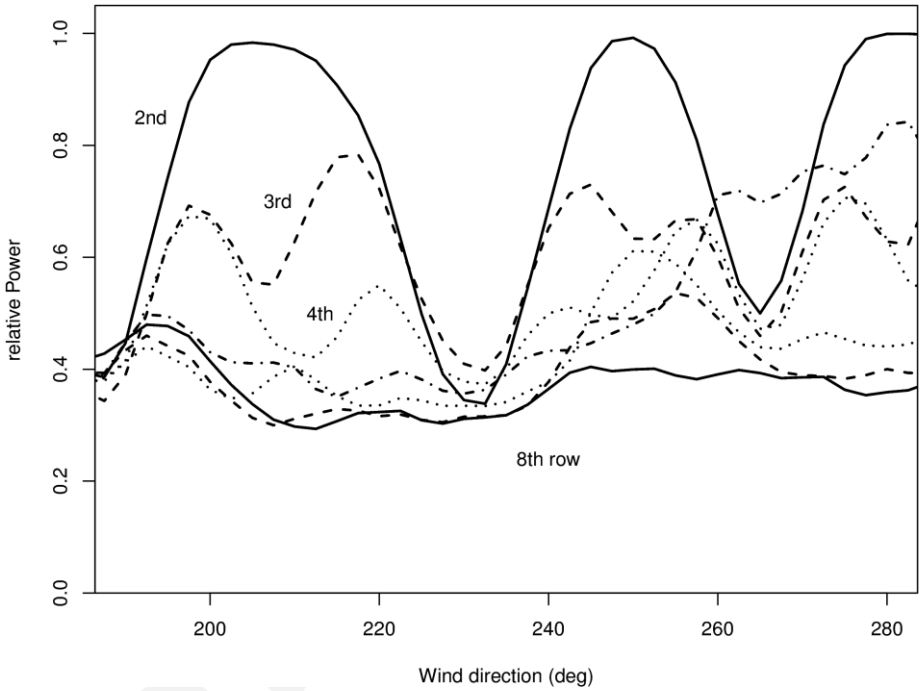

Figure 2. Wind directional dependence of relative power.

The sensitivity of turbines in the second and further rows to the wind direction is shown in Figure 2, in which the power output of turbines compared to the front turbine is shown against the wind direction, where the wind direction of 230º is the case where the turbine row is fully aligned with the upstream wind. Due to the nonlinear nature of the turbine's power curve, the analysis centres on the wind speed range where the power output changes with speed, that is between the cut-in wind speed and the rated wind speed. In this case, the turbines only produce between 30 and 40% of the front turbine. The wind directions of 105º and 250º are those where the wakes from the front row miss the turbines in the second row but those in the third row are now directly downwind of the front row turbine. These observations clearly show that the reduced velocity in the wind turbine wake has a strong effect on the productivity of a turbine in the wake. Some have suggested that the overall wind farm might actually generate more power if the front turbines are operated somewhat below their optimum conditions which allows the other turbines to produce more [87][74].

Another feature evident in Figure 2, very much in common with observations from other wind farms [8][9], and numerical models such as Churchfield et al [22], is that once the available power has been reduced by a second turbine, it does not get reduced much further for a third turbine. In fact, in some cases, the third turbine performs better than the second, as is the case here for full alignment: the turbines in 3rd to 5th row perform noticeably better than the 2nd turbine. This phenomenon is currently explained such that the turbulence induced by turbines – especially those

operating in the turbulent inflow conditions of a wake – helps to disperse the wake much better than a wake with a lower turbulence level. However, it has to be borne in mind that other studies present a continued decrease of the average performance for turbines deeper into the wind farm array, a phenomenon usually referred to as the "deep array effect". To interpret these plots one has to bear in mind that they have to be obtained through averaging of wind speeds, weather conditions and, most importantly, over a finite wind direction sector. For example, Figure 2 was obtained by averaging over a ±2.5º window, whereas the deep array effect becomes visible when averaging over a larger sector, such as ±10º or even more. Considering that the actual wind is never fixed in speed and direction throughout the array over the averaging period of an individual observation (typically a few minutes), and that the nominal wind direction is determined either from a single point or as an average across the array, it is not clear how large the averaging sector should be to give the most appropriate representation of effect.

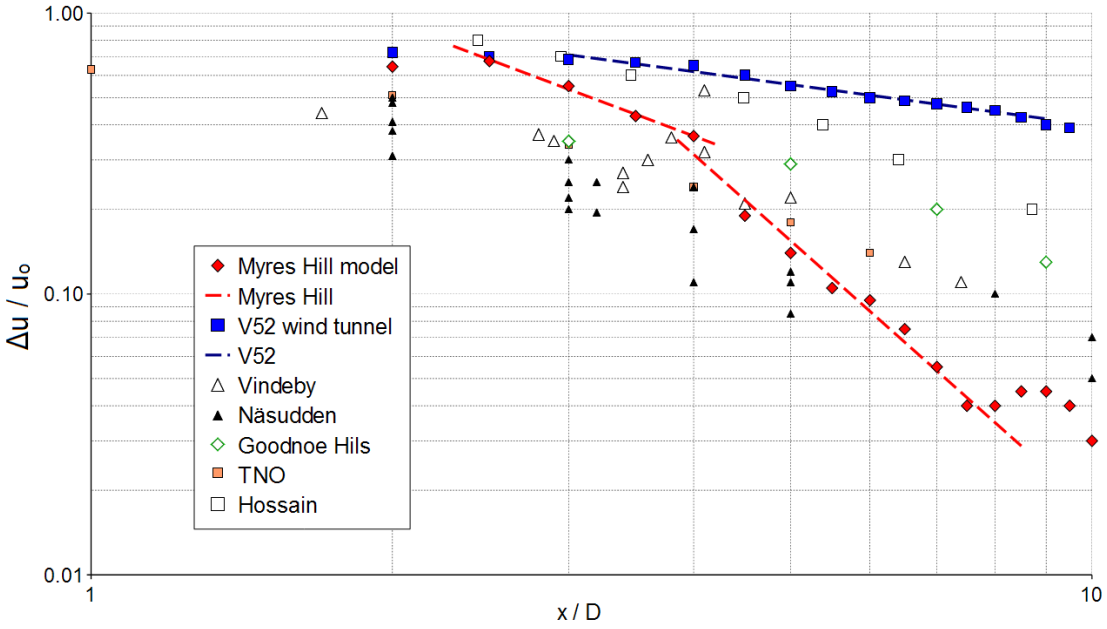

Figure 3. Environmental effects in single-turbine wake recovery, from Creech et al [27].

2.3 Individual turbine wake recovery

Again, from field measurements, wind tunnel tests and numerical models, it is well known that upstream turbulence strongly affects the decay of the wake [27], where a higher level of turbulence helps to erode the wake faster. This is illustrated in Figure 3, in which the decay of the wake is plotted for a number of different situations, including a direct comparison between a measured wake behind an 950kW turbine and a computational model of it in situ. The exact nature and processes by which the upstream turbulence affects the wake recovery is not yet well understood and requires detailed experiments and numerical models; while the induced wake turbulence helps with the wake recovery and thereby power output, at the same time it increases fatigue loads on the turbine by up to 80% [72], which would be expected to shorten the life span of turbine blades substantially.

Finally, some have observed that the relative yaw position of the turbines also affects the performance of the downstream turbine [1][32].

2.4 Outline

This short overview serves to highlight the fact that different fluid dynamical processes associated with turbine wakes have several very strong effects on other turbines in a wind farm, with

implications for the life time of turbine blades, the optimum design of wind farms, and the optimum operation of wind farms. It is therefore very important to build up a good understanding of these processes and to develop a range of models, some of which would have to be fairly simple to be feasibly incorporated into the planning or operational tools and some which would have to try to explore the full dynamics at the expense of a high complexity of these models. A key earlier review of wind turbine and wind farm wake modelling was that by Crespo, Hernández and Frandsen in 1999 [30]. Since then, computing power of workstations and clusters has increased tremendously, opening up the possibilities of resolving more and more detail in direct computational fluid dynamics (CFD) simulations. Even though, it is still impossible to configure a CFD model to include a number of wind turbines represented as rotating solid boundaries in a computational domain representing the surrounding topography. At the same time, the number of large wind farms has, and is continuing to, increase rapidly with a need to be able to represent wake effects in a relatively simple way, both for wakes from individual turbines on other turbines in the wind farm and for the effect the wind farm as a whole has on its environment, including possible wind farms downstream of other wind farms. Reflecting this, there were a number of activities noteworthy at the time of this entry, including the EUROMECH colloquium 508 on *Wind Turbine Wakes* in 2009 [49], and the IEA WAKEBENCH initiative inaugurated in 2010 [94].

In line with the variety of methods used, the remainder of the will introduce a hierarchy of models, starting with simple empirical models in section 3, and gradually building up to models of the full time-varying three-dimensional fluid dynamics of the flow around a single wind turbine or a wind farm. After a section introducing the principles of Computational Fluid Dynamics in section 4, section 5 introduces the methods to model the effect of wind turbines on the fluid in a CFD model. Section 6 then describes CFD-based wind turbine and wind farm models which are finally compared in section 7.

3 Empirical methods to estimate wake recovery

For many years, the wake decay has been parameterised in flow models of proposed wind farms through a small number of models or assumptions, most notably using the Park model [41][47] or through Eddy Viscosity [2]. A systematic survey has compared a range of these approaches with SODAR measurement from the Vindeby offshore wind farm [7] which highlighted the spread of results and the need to both interpret their results accordingly and to develop more accurate methods.

Jensen's Park model is a simple method based on momentum conservation and assuming entrainment of free-stream air surrounding the wake into the wake. In the simple models, a constant wake entrainment factor α is used and the wake expands linearly with distance, x, behind the rotor of radius R_T, given by $r_w = R_T(1+\alpha x)$. The velocity in the wake as a function of downstream distance, x, from the rotor is given in [41] as

(1) $$u(x) = u_0\left[1-2a\left(1+\alpha\left(\frac{x}{r_w}\right)\right)^{-2}\right]$$

Where a is the axial flow induction factor as used in the actuator disk theory, and related to the thrust coefficient of the turbine as $C_T = 4a(1-a)$. The wake entrainment factor depends on the free-stream turbulence level and velocity shear. For example, from Mosetti et al [62] it can be empirically calculated from the hub height, z_{hub}, and the surface roughness, z_0, as

(2) $$\alpha = \frac{0.5}{\ln\left(z_{hub}/z_0\right)}$$

In practice, this approach is implemented on the basis of the thrust coefficients for the wind turbine as supplied by the manufactures and using recommended entrainment or wake decay coefficients, for example WAsP [7] uses

(3) $$u(x) = u_0\left[1-\left(1-\sqrt{1-C_T}\right)\left(\frac{D}{D+2k_w x}\right)^2\right]$$

where the D is the rotor diameter and k_w the wake decay coefficient, with suggested values of k_w= 0.05 for offshore, and 0.075 for onshore cases.

A variant of the Jensen model is the Frandsen model [37] which does not assume a linearly expanding wake but specifies a wake diameter based on the thrust coefficient of the turbine and a wake entrainment factor as

(4) $$D_W = \left(\beta^{k/2} + \alpha\frac{x}{D}\right)^{-1/k}$$

with $\beta = \frac{1+\sqrt{1-C_T}}{2\sqrt{1-C_T}}$, the constant α typically recommended to be α = 0.05 and k between 2 and 3, usually taken as k = 3 (see [37]), and a wake velocity of

(5) $$u(x) = u_0\left[1-\frac{1}{2}C_T\left(\frac{D}{D_W}\right)^2\right]$$

In the application of this method for an array of turbines, the wake behind each individual turbine is allowed to expand until it either reaches the ground or meets another wake. Once this happens, the wakes are merged while the total momentum deficit is conserved.

The Eddy Viscosity approach originally developed by Ainslie [2] uses the momentum equations with an eddy viscosity term replacing the molecular diffusion for axisymmetric wake flow. As Crespo et al [30] have pointed out that one weakness of the axisymmetric wake flow is that it cannot resolve wind shear caused by surface roughness or atmospheric stability. The UPMWAKE model [28][29] was developed to allow for a turbine to be situated in a non-uniform flow. This model assumes an initial analytical velocity profile which represents the effect of atmospheric stability, as given by the Monin-Obukhov length, and the surface roughness, which is then perturbed by the wind turbine using RANS computational fluid dynamics modelling with a k-ε turbulence model. A recent comparison showed that both the Park models and the eddy viscosity models consistently overestimate the electricity production from large wind farms, where most of the error arose form turbines in the fourth row relative to the wind and further [11].

One aspect which all methods struggle with is that even the freestream wind is never constant, and the fluctuations in wind speed and direction continually affect not only the generation of the wake at the turbine but also the advection of the developing wake downstream. As a result, the wake is never a smoothly expanding wake along a straight trajectory but it meanders in the lateral direction.

One simple approach to capture the effects of wake meandering is to superimpose a simple wake model on a wind which is fluctuating in direction, for example using a stochastic model [48][50].

4 Computational fluid dynamics

As computational fluid dynamics techniques represent a very active area of much of recent wake modelling research, this section is devoted to outlining the most common methods used, including finite element, finite volume, finite difference and vorticity methods; turbulence modelling is also discussed in brief. Both vector and Einstein notation are used below to provide maximum clarity.

4.1 Basic equations

At its simplest level, computational fluid dynamics problems for wind energy problems must solve the equations for incompressible Newtonian fluids, ie. the momentum and continuity equations, which can be written in Einstein notation respectively as

(6) $$\rho\left(\frac{\partial u_i}{\partial t}+u_j\frac{\partial u_i}{\partial x_j}\right)=-\frac{\partial p}{\partial x_i}+\mu\frac{\partial}{\partial x_j}\left(\frac{\partial u_i}{\partial x_j}\right)+F_i$$

And

(7) $$\frac{\partial u_i}{\partial x_i}=0$$

Where u_i represents the velocity field, p the pressure field, ρ the density of air, μ the molecular viscosity of the air, and F_i any body forces acting on the fluid, such as gravity.

In addition to these, boundary conditions may be applied, which can take the form of Dirichlet conditions for a given field ψ:

(8) $$\psi=a$$

Von Neuman, for co-ordinate components x_i:

(9) $$\frac{\partial\psi}{\partial x_i}=a$$

Or Robin conditions, a compound of the two:

(10) $$\frac{\partial\psi}{\partial x_i}+b\psi=a$$

Where a and b are given constants; ψ can represent either the velocity components u_i or the pressure p.

The momentum equation is a second-order, partial differential equation, coupled to the continuity equation. For many realistic scenarios, solving both these simultaneously and explicitly is impossible. In recent decades, there have been efforts to solve them numerically; we will cover the most common methods of discretising and solving these equations below.

4.1.1 Finite difference

Finite difference techniques have long been used in computational fluid dynamics, being one of the least complex to implement. Here the simulation domain is represented by a regular grid, with the velocity field defined at regular intervals; often a staggered grid approach is implemented, so that the pressure terms are defined in the centre of each grid cell, as shown below in Figure 4. A two-dimensional finite difference grid, courtesy of Fletcher [36].

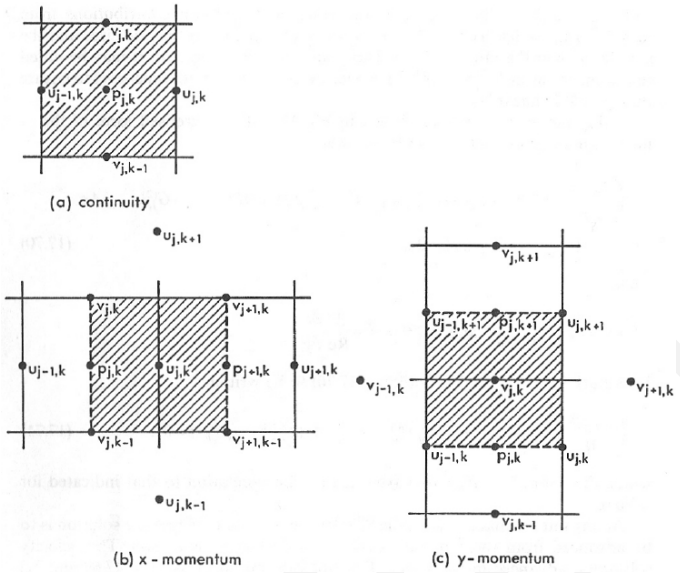

Figure 4. A two-dimensional finite difference grid, courtesy of Fletcher [36].

The finite difference approach has the benefit of being straightforward to assemble into matrix form, given the spacing between each grid-point which does not change with time. However, this also means that problems with complex geometries are poorly represented, and that grid resolution cannot be arbitrarily concentrated to better resolve local flow structures.

Coupling pressure and velocity

As pressure and velocity are coupled via the momentum equation (6) and mass continuity equation (7), at each time-step these must be both be solved for whilst ensuring continuity. A common technique for doing so was first introduced by Patankar and Spalding [66] in their SIMPLE algorithm (Semi-Implicit Method for Pressure Linked Equations), whereby pressure and continuity terms are linked semi-implicitly. Before the first time-step, the pressure values on the grid are initialised to some value, usually to zero, then the values for the velocity and pressure are iteratively updated, until both $\underline{u}$ and p converge towards stable values. The steps of the iteration are as follows (from Fletcher [36], p362-365):

1. Calculate the guess for the correct value for the velocity field $\underline{u}^*$
2. Obtain the correction to the pressure δp
3. Calculate of the velocity correction $\underline{u}^c$
4. Update the pressure via $p^{n+1} = p^n + \alpha_p \delta p$, where α_p is the pressure relaxation parameter.
5. Set $\underline{u}^{n+1} = \underline{u}^* + \underline{u}^c$ ready for the next iteration.
6. If the velocity and pressure fields have not converged, go to step 1.

SIMPLE methods are typically slow to converge, and so two alternative schemes were developed. These are SIMPLEC [33] which approximates terms in the pressure correction equations previously neglected in SIMPLE, and SIMPLER [67], which solves the pressure correction term first so that it can be used to correct the velocity field to satisfy continuity. For further reading on linking pressure-velocity, see Ferziger et al [35] section 7 and Fletcher [36] section 17.2.3. Note, these methods are not exclusive to finite difference techniques, and are also used in finite volume and finite element formulations.

4.1.2 Finite volume

In finite volume methods, the simulation volume is divided into small, finite control volumes (CVs) which represent cells on a mesh, or grid. The nodes are defined in the centre of these CVs. The differential equations governing the flow, eg. the momentum and continuity of mass equations, are integrated over each control volume. The advantage this approach is that by design it satisfies the conservation of mass and momentum in every CV, even on relatively coarse grids. It is for this reason that it is a popular technique with commercial computational fluid dynamics software packages such as ANSYS CFX [5]. The starting point is to take the integral, rather than differential, form of the momentum and conservation equations, which for an incompressible fluid are:

$$\rho \frac{\partial}{\partial t}\int_V u_i dV = \int_V \left[-\frac{\partial p}{\partial x_i} - \left(\frac{\partial u_i}{\partial t} + u_j \frac{\partial u_i}{\partial x_j} \right) + \mu \frac{\partial}{\partial x_j}\left(\frac{\partial u_i}{\partial x_j} \right) + F_i \right] dV \tag{11}$$

and

$$\int_S u_i \, n_i \, dS = 0 \tag{12}$$

Where V represents the volume of a particular finite volume, S its surface, and n_i is a vector normal to that surface. This equation guarantees that for each finite volume, momentum is conserved. For more on finite volume techniques an excellent introduction can be found in Ferziger [35].

4.1.3 Finite element

Finite element methods (FEM) have come to the fore recently particularly in oceanographic modelling [53][63][65], due to their ability to handle unstructured meshes, an ability which allows them to adapt to models with complex boundaries, such as irregular terrain or bathymetry. An excellent example of this would be the tidal simulation of Venetian Lagoon by Canu et al [18], shown in Figure 5, which shows the unstructured triangular mesh fitted to the coastline, and its resolution concentrated in particular areas of interest.

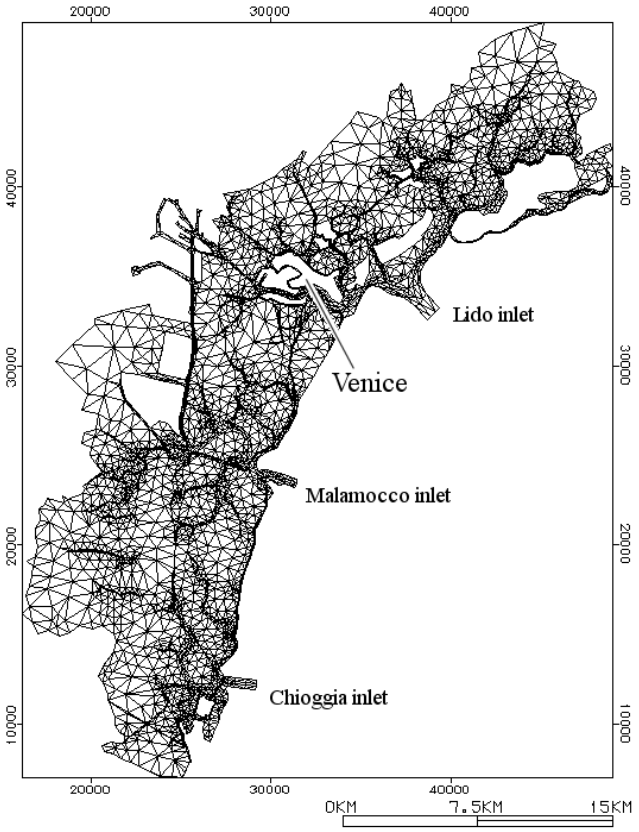

Figure 5. Finite element simulation of the Venetian lagoon, courtesy of Canu et al [18].

In finite element methods, the simulation domain is discretised into elements which in two dimensions can be triangles, squares or hexahedra, or in three dimensions tetrahedral or cuboids. Triangular and tetrahedral meshes are common, due to being simple to implement in unstructured meshes. Each element is defined by the nodes, eg. the values of momentum, pressure etc. at the corner of each element; nodes are shared with neighbouring elements. Each field defined within an element using basis functions, so the velocity and pressure fields can be written as

$$\underline{u} = \sum_{n=1}^{N} \Phi_n \underline{u}_n \tag{13}$$

$$p = \sum_{n=1}^{N} \Psi_n p_n \tag{14}$$

Where N is the number of mesh nodes, with Φ_n and Ψ_n the basis functions for velocity and pressure respectively. The above equations are the global representation of velocity and pressure; in finite element analysis, we start with a local representation, with interpolation of each occurring within each element. These can be of any order but a common choice is linear for both, often referred to as a P1P1 element pair (first order pressure, first order velocity). Figure 6 illustrates this with the velocity u on a one-dimensional line discretised into three elements, with four nodes in total. It shows how the velocity field between nodes 1 and 2 (in b) is the sum of the two interpolation functions, $\Phi_1^{(1)}$ and $\Phi_1^{(2)}$, within element $e=1$ (in a). As one of the most straightforward implementations, it is less computationally expensive than higher order formulations. Through the Galerkin method, the local matrices are assembled into a global form of the momentum and continuity equations to be solved. A thorough description of the Galerkin

method, and computational fluid dynamics using finite element analysis in general can be found in many fluid dynamics books, such as Chung [21].

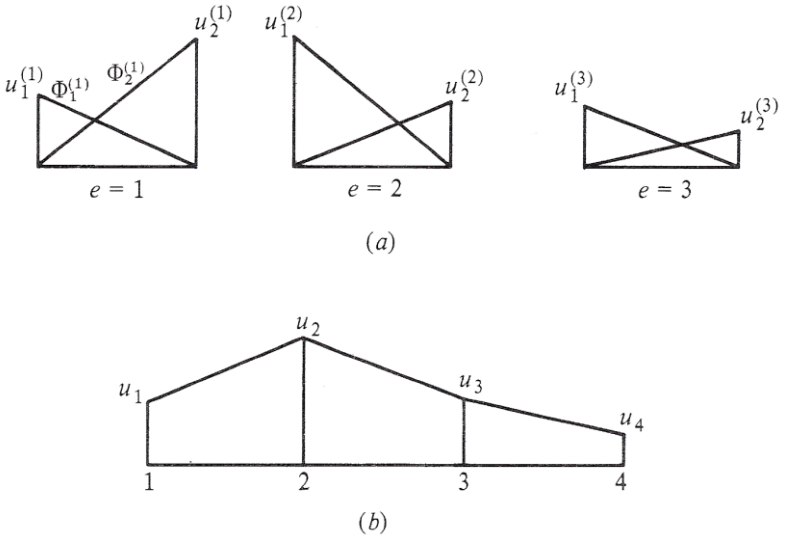

Figure 6. a) Local and b) global linear interpolation for u, courtesy of Chung [21].

As stated previously, the key advantages of finite element analysis methods is their ability to handle irregular terrain, and so their rise in physical oceanographic modelling. This very same virtue allows them to be adapted to modelling wind farms in hilly areas, and has been used by Creech et al [27] for this purpose. However, their main disadvantage is that they do not naturally preserve the continuity of mass, as finite volume techniques do. To do so requires further controls, as has been implemented by Cotter [96].

4.1.4 Vorticity equation

Since the lift F_L is generated by an ideal aerofoil is given by the circulation, Γ, induced in the flow by the aerofoil such that $F_L = -\rho u_0 \Gamma$, it is intuitive to model the evolution of the wake based on the conservation equations for vorticity rather than momentum. This can be implemented in an Eulerian approach by solving the vorticity equation on a domain-filling mesh or grid, as found in Hansen et al [39], which in the most basic form with only molecular diffusion is

(15) $$\frac{D\underline{\omega}}{Dt} = \frac{\partial \underline{\omega}}{\partial t} + (\underline{u}\cdot\nabla)\underline{\omega} = (\underline{\omega}\cdot\nabla)\underline{u} - \underline{\omega}(\nabla\cdot\underline{u}) - \upsilon\nabla^2\underline{\omega}$$

or, allowing for a turbulent eddy viscosity, υ_t, and body forces $\underline{f}$ (Vermeer et al [93]),

(16) $$\frac{\partial \underline{\omega}}{\partial t} + \nabla\times(\underline{\omega}\times\underline{u}) - \upsilon\nabla^2\left[\left(1+\frac{\upsilon_t}{\upsilon}\right)\underline{\omega}\right] + \nabla\times\underline{f} + \underline{Q}_\omega$$

on a domain-filling mesh or grid, where $\underline{\omega} = \nabla\times\underline{u}$ is the vorticity vector and υ the kinematic viscosity; continuity completes this through $\nabla\cdot\underline{u} = 0$. These two conditions can be combined into a single set of Poisson equations as $\nabla^2\underline{u} = -\nabla\times\underline{\omega}$.

While it appears a very attractive approach by eliminating the pressure term and implicitly satisfying continuity, it is not well-suited for high Reynolds number cases or complex geometries [40].

4.1.5 Vortex particle methods

Alternatively, a Lagrangian method such as the vortex particle method can be adopted [93][99], where the motion and evolution of a large number of individual vortices are computed based on Biot-Savart's law of the velocities induced by a vorticity distribution as

$$\underline{u}(\underline{x}') = \frac{1}{4\pi}\iiint \frac{\underline{\omega}\times(\underline{x}-\underline{x}')}{|\underline{x}-\underline{x}'|^3} d\underline{x} \quad (17)$$

Where the integration has to be carried out over the entire part of the domain which has non-zero vorticity.

Using this the global flow field is then determined as the superposition of the external flow, and the flow induced by the vorticity generated by the turbine blades. This superposition usually implies that the external flow has zero vorticity and simply acts as a background flow to advect the vortices. A number of studies have used this approach for a hierarchy of complexity but always requiring a prescribed vorticity generated by the turbine rotor. Once the vorticity is specified, the transport of the vorticity can be calculated either in a prescribed wake or a free wake.

In the simplest vortex models the rotor is represented by a hub vortex and a set of vortex rings, as if the rotor had an infinite number of blades, such as is found in Miller [61] and Øye [64]; the former with a fixed wake and the latter including a wake expansion. Despite, or maybe because of their simplicity, these models were able to simulate the wake reasonably well.

To move from an idealized rotor disk to a rotor with a finite number of specific blades, it is necessary to prescribe the vortex lines generated from each blade section rather than the azimuthally averaged vorticity ring. The most common approach is to use the vorticity generated by the bound circulation as specified through the Kutta-Joukowsky theorem. As this assumes two-dimensional and steady flow over an aerofoil section, this circulation has to be corrected to account for transient effects, such as dynamic stall [51], and three-dimensional effects, such as rotational augmentation [75]. Further developments of this approach include the so-called boundary integral equation method (BIEM) [25], in which the actual rotor blade geometry is represented through vorticity sources at the surface in addition to the vorticity doublets, while the vorticity away from the surfaces is described by doublets alone.

The vorticity generated by the turbine is then used in a model which either prescribes the wake structure [23][24] or has a free wake [6]. The prescribed vortex method, where the position of each vortex is prescribed, has the advantage of being computationally very cheap and robust but are only valid if their position is adequately prescribed, which limits this to fairly simple and well-known situations. On the other hand, the free vortex method is not restricted to cases where the wake is known but includes the calculation of the wake velocities from the basic equations; an example of this is shown in Figure 7(a) and compared to a commercial RANS CFD package in Figure 7(b). The cost of this is that the integration of the Biot-Savart equation must be calculated for each point in the domain. Furthermore, the calculations are prone to computational instability from the singularities which arise when two vortices are approaching each other.

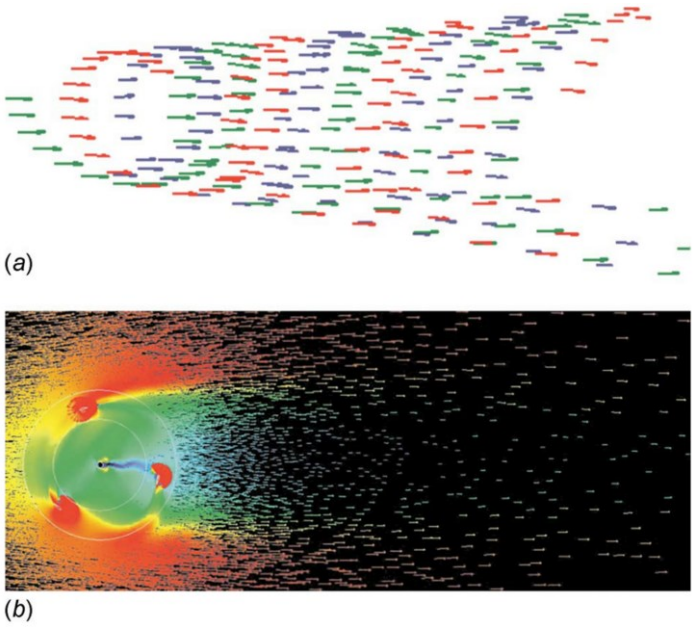

Figure 7. Comparison of the wake velocities calculated using (a) a Discrete Vortex method and (b) a commercial RANS CFD package (source: Li and Çalişal [55]).

4.2 Turbulence

Most of the flows considered in wind turbine modelling are unsteady, turbulent flows, and so cannot be considered laminar. As such, turbulence must be taken into account for accurate wake simulation. For practical reasons, it is often treated with a degree of implicitness – the most common formulations being the fully implicit Reynolds-Averaged Navier-Stokes, or the semi-explicit Large Eddy Simulation method.

4.2.1 Reynolds-Averaged Navier-Stokes

Reynolds-Averaged Navier-Stokes (RANS) takes the approach that unsteadiness in the flow is considered fluctuations about a steady state. This means that there is no distinction between above grid or sub-grid turbulence, and that both are implicitly modelled. Whilst this approach cannot be expected to predict all types of turbulence flow accurately, RANS is a relatively inexpensive technique, and so a popular choice for modelling fluid dynamics problems.

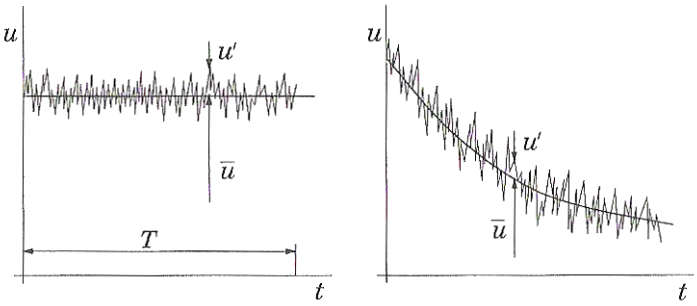

Figure 8. Time averaged velocity for statistically steady flow (left) and unsteady flow (right) with ensemble averaging. Courtesy of Ferziger and Perić [35].

The velocity and pressure fields can be separated into steady and fluctuating components, as shown in Figure 8:

(18) $$\underline{u} = \underline{\overline{u}} + \underline{u'}$$

(19) $$p = \overline{p} + p'$$

Where $\underline{\overline{u}}$ and $\overline{p}$ represented the time and ensemble-averaged values, with $\underline{u'}$ and p' the fluctuations. The momentum and continuity equations for an incompressible Newtonian fluid then become:

(20) $$\rho \frac{\partial \overline{u}_i}{\partial t} + \frac{\partial}{\partial x_j}\left(\rho \overline{u}_i \overline{u}_j + \rho \overline{u_i' u_j'}\right) = -\frac{\partial \overline{p}}{\partial x_i} + \frac{\partial \overline{\tau}_{ij}}{\partial x_j}$$

(21) $$\frac{\partial \overline{u}_i}{\partial x_i} = 0$$

Where $\overline{\tau}_{ij}$ represents the mean viscous stress tensor, ie.

(22) $$\overline{\tau}_{ij} = \mu\left(\frac{\partial \overline{u}_i}{\partial x_j} + \frac{\partial \overline{u}_j}{\partial x_i}\right)$$

From the above equations, of particular interest is the term $\rho \overline{u_i' u_j'}$ in equation (20), which represents the Reynolds stress, ie. the fluid stress due to the fluctuations of the flow from the steady state. This must be solved implicitly, as it cannot be represented explicitly in terms of the mean values. Boussinesq postulated [76] that the Reynolds stress could be formulated as

(23) $$-\rho \overline{u_i' u_j'} = \mu_t\left(\frac{\partial \overline{u}_i}{\partial x_j} + \frac{\partial \overline{u}_j}{\partial x_i}\right) - \frac{2}{3}\rho \delta_{ij} k$$

Where μ_t is the eddy viscosity, δ_{ij} is the Kronecker delta, and k is the turbulent kinetic energy. μ_t represents the additional viscosity due to fluctuations (ie. eddies) about the mean velocity values, and k the additional kinetic energy that arises because of them. Solving for μ_t and k closes the turbulence, and common approaches to do this are the $k-\varepsilon$ and $k-\omega$ models [52] [95].

4.2.2 Large-Eddy Simulation

Large eddy simulation (LES) takes the approach of resolving turbulence in a partially statistical, partially explicit manner. The turbulence is separated into large and small scales by applying a filter to the velocity field, so that in numerical simulations flow features larger than the grid resolution are resolved explicitly, whilst features smaller than the grid resolution are resolved implicitly. We define each component of the filtered velocity field as

(24) $$\overline{u}_i = \int G(x, x') u_i(x, x')\, dx'$$

Where $G(x, x')$ is the filter kernel. This filter is a localised function and has an associated length scale, Δ, which represents the division between small-scale and large scale turbulence. Examples of possible filter kernels are a simple local average or a Gaussian. For an incompressible fluid, the Navier-Stokes equations become

(25) $$\rho\left(\frac{\partial \overline{u}_i}{\partial t}+\overline{u}_j\frac{\partial \overline{u}_i}{\partial x_j}\right)=-\frac{\partial p}{\partial x_i}+\mu\frac{\partial}{\partial x_j}\left(\frac{\partial \overline{u}_i}{\partial x_j}\right)-\frac{\partial \tau_{ij}^{\Delta}}{\partial x_j}$$

(26) $$\frac{\partial \overline{u}_i}{\partial x_i}=0$$

The additional term $\nabla\cdot\tau^{\Delta}$ represents the additional stress due to small eddies that are not resolved explicitly, and the sub-grid stress tensor is defined as

(27) $$\tau_{ij}^{\Delta}=\overline{u_i u_j}-\overline{u}_i\overline{u}_j$$

τ_{ij}^{Δ} is needed to close equation (25), and so a SGS model is required. A common choice is the Smagorinsky model, which defines the SGS stress as

(28) $$\tau_{ij}^{\Delta}=2\mu_t\overline{S}_{ij}$$

Where μ_t is the sub-grid eddy viscosity, and $\overline{S}_{ij}$ is the strain rate of the resolved velocity field. The eddy viscosity term is then defined as

(29) $$\mu_t=C_S^2\rho\Delta^2\left|\overline{S}\right|$$

Where C_S is a parameter to be defined, and $\left|\overline{S}\right|=\sqrt{\left(\overline{S}_{ij}\overline{S}_{ij}\right)}$. Estimates for isotropic turbulence usually give $C_s\approx 0.2$; however the Smagorinsky constant, as it is often known, is often *not* constant but varies with the type of flow, and can be a function of the Reynolds number as well as other flow parameters.

5 Rotor modelling techniques

Several approaches exist to modelling with the turbines within simulation, most of which use indirect methods to represent the turbine blades. In principle, it is possible to simulate the full fluid dynamics by specifying the entire turbine through solid boundaries in the CFD domain and expect the boundary conditions and shear forces to lead the flow to respond to the turbine blade forces. However, this requires considerable computing resources; in contrast, indirect methods afford turbine models a degree of simplicity, so making them cheap from a computational perspective. Within these models, there are increasing degrees of complexity, from the simpler generalised actuator discs, to actuator lines and surfaces (see Figure 9); these come with an associated rise in processing requirements.

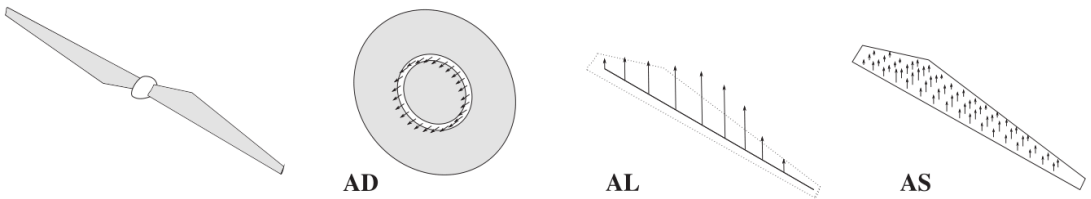

Figure 9. Indirect representations of turbine blades: actuator disc (AD), actuator line (AL), and surface (AS). Sanderse et al [73].

5.1 Actuator discs

5.1.1 Uniform thrust

The simplest representation of the turbine is by a disc of uniformly distributed thrust, which has a surface area A. The total force on the fluid, opposing the direction of flow, is specified as

(30) $$f_t = -\frac{1}{2} C_T \rho u_0^2 \pi R^2$$

Where u_0 is a reference wind speed at hub-height some distance upwind, C_T is the thrust co-efficient for turbine, usually a function of u_0 and R the rotor radius. The calculation of u_0 can be problematic, especially in simulations with complex flow, from upwind turbines or irregular terrain. Finding u_0 is not straightforward due to the effect of the thrust on the flow, and so the relation $u_0 = u_{local}/(1-a)$ is used, where a is the axial induction factor and u_{local} the local flow field. To determine a, Prospathopoulos et al [70] presented at iterative procedure whereby an initial guess at u_0 is made to determine C_T. Taking u_{local} from the flow field round the disc, we can find a, and so a new value for u_0. This is repeated until convergence is achieved. A slightly different method was used by Calaf [17] and Meyers [58], replacing u_{local} with $\overline{u}_{disc}$, an average calculated across area of the disc. This was used to directly calculate the backthrust, ie.

(31) $$f_t = -\frac{1}{2} C_T' \rho \overline{u}_{disc}^2 \pi R^2$$

Where the modified thrust coefficient $C_T' = C_T/(1-a)^2$. Instead of using an iterative solution, typical values for C_T and a were taken the Wind Energy Handbook [13] , giving $C_T' = 4/3$.

5.1.2 Blade element momentum theory

A further refinement to the actuator disc is to consider annular variations across the disc, rather than uniform, by incorporating parts of blade element momentum (BEM) theory to calculate of lift and drag forces. Although disc representation means the blades cannot be discrete, the influence of the blades is spread azimuthally in infinitely thing rings centred on the hub. The lift and drag forces per span wise unit length on a blade section are commonly written as

(32) $$\underline{f}_{2D}(\underline{x}) = \frac{1}{2} \rho u_{rel}^2 c \left[\underline{e}_L C_L + \underline{e}_D C_D\right]$$

Where C_L and C_D are the lift and drag coefficients, which vary with the angle of attack α and the Reynolds number Re, $\underline{e}_L$ and $\underline{e}_D$ are unit vectors in the direction of lift and drag respectively, u_{rel} is the local relative speed of the air to the blade surface, and c is the chord length of the blade at distance r from the hub. Note, the inclusion of c allows blade geometry variation.

The determination of C_L and C_D can be made from lift/drag co-efficient graphs, plotting the coefficient graphs as a function of α for a variety of Reynolds numbers. Graphs for aerofoils commonly used in wind turbines, such as the NACA 63- and 64- series, are readily available [12]. As such graphs to not incorporate unsteady effects, typical in unsteady flow, Masson et al [57]

incorporated a dynamic stall model to give accurate aerofoil performance with fluctuating values of attack.

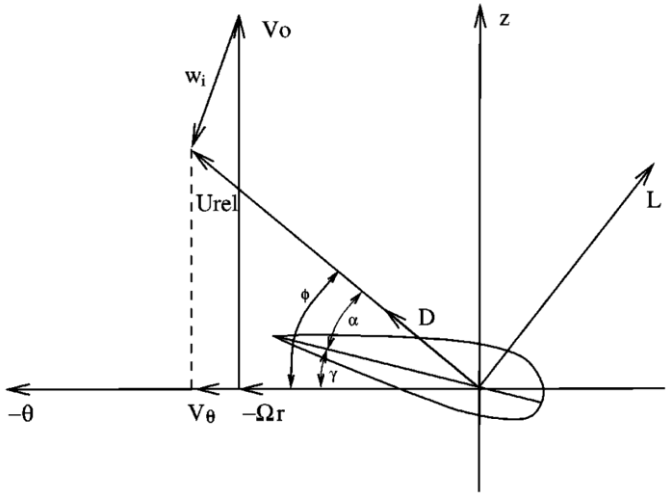

Figure 10. Cross-section of an aerofoil, showing the direction of the lift and drag forces, the direction of u_{rel}, the angle of attack α, and the local pitch angle γ. From Sorensen et al [82].

The angle of attack α can be determined in several ways. Shen and Hansen look at the flow field upwind of the rotor [77]; another approach is to derive α from $\overline{u}_{disc}$, the angular velocity of the blades, and local blade twist [27]:

(33) $$u_{rel} = \sqrt{(r\omega)^2 + \overline{u}_{disc}^2}$$

This can present problems under high rotor loading where $u_0 >> \overline{u}_{disc}$; this is similar to an issue addressed in actuator discs by others [17][58][70].

Recently, reactive turbine models have coupled lift and drag forces to turbine models, to simulate the unsteady behaviour of rotors and mimic power generation through a generator (see Creech et al [27]). As the force on the fluid at each point on the actuator disc is known at each time-step, then the total torque acting on the fluid, τ_{fluid}, is also known. This must by necessity be balanced by the torque accelerating the blades, and the resistive torque of the generator, such that

(34) $$\tau_{fluid} = -(\tau_{blades} + \tau_{gen})$$

If we choose a simple approximation of a generator, and assume that it is a direct function of angular velocity [89], then we can write

(35) $$\tau_{gen} = k\omega^2$$

Where k is a constant defined from the performance specifications of the turbine, then we can also calculate the power generated

(36) $$P = \tau_{gen}\omega^2$$

Now that both the generator and fluid torque are known, the torque accelerating the blades can be determined, and if the momentum of inertia of the blades can be calculated, so can the angular acceleration of the rotor. In this way, turbine performance and blade loading can be entirely dynamic, which is useful for Large Eddy Simulation turbulence models. Note that this or similar approaches can also be applied to the other actuator methods outlines below, and have indeed been by Churchfield et al [22], who applied a torque controller based upon a reference model at NREL for a 5 MW turbine [45].

5.1.3 Numerical discretisation

As simulations will be either grid or mesh based, the disc thrust will likely be spread over several cells. This necessitates the use of a kernel to spread the forces axially across a volume, ie.

(37) $$\underline{f}_{mesh} = \underline{f}_{disk} \otimes \eta_{\varepsilon}$$

Sørensen et al [81] proposed a Gaussian kernel, η_{ε}, where the parameter ε controls the standard deviation and so the 'smearing' of the thrust; larger values of ε give greater stability, smaller values greater accuracy. Others simply spread the thrust evenly in the axial direction across a cylindrical volume [27] making the kernel even and $\underline{f}_{mesh}$ dependent on the thickness of the cylinder.

5.2 Actuator lines and surfaces

Further accuracy can be achieved through using the actuator line method, first described by Sørensen and Shen [82]. Here, the forces on the fluid are concentrated around lines which represent the blades. In cylindrical co-ordinates (θ, r, z) these are

(38) $$f_{\theta} = \frac{\rho c u_{rel}^2}{2r\, d\theta\, dz}\left(C_L \sin\phi - C_D \cos\phi\right)$$

(39) $$f_{z} = \frac{\rho c u_{rel}^2}{2r\, d\theta\, dz}\left(C_L \sin\phi + C_D \cos\phi\right)$$

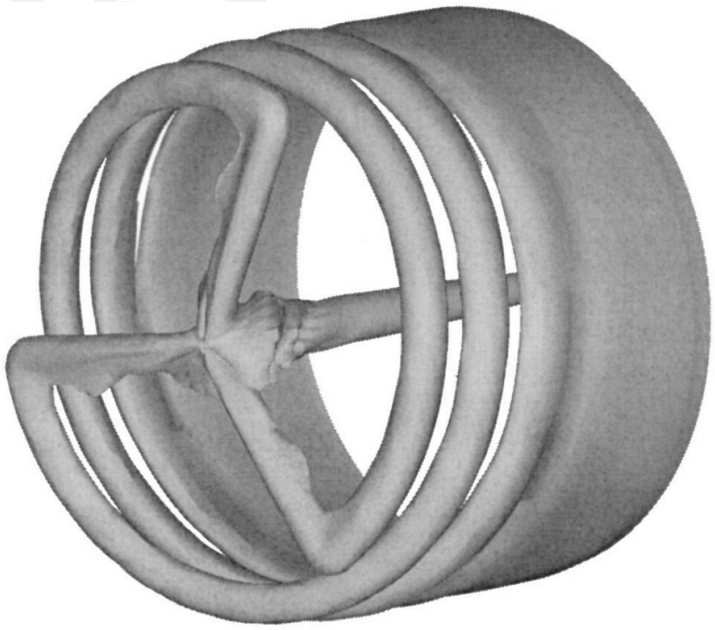

Figure 11. Vorticity field from an actuator line simulation at freestream wind speed of 10m/s (Sørensen et al [82]).

A regularisation kernel is applied as before in equation (37), however the kernel is now a Gaussian function of the distance from the force points on the rotor blades, ie.

$$\eta_\varepsilon(r) = \frac{1}{\varepsilon^3 \pi^{3/2}} \exp\left(-\frac{r}{\varepsilon}\right) \tag{40}$$

Where r is the distance from the force points. The total force on three bladed turbine is then written

$$\underline{f}_e(\underline{x}) = \sum_{i=1}^{3} \int_0^R \underline{f}_{2D}(r)\, \eta_\varepsilon\left(\left|\underline{x} - r\underline{e}_i\right|\right) dr \tag{41}$$

Where $\underline{e}_i$ is a unit vector in the direction of blade i.

Sørensen et al [82] ran axisymmetric simulations of a Nordtank turbine in a wind tunnel, and found good agreement with measured power output at a varied wind speeds, and that tip-shed vortices were being produces, which quickly diffused into continuous vortex sheets. Despite being numerically intensive compared to other techniques, more recently actuator line methods have been applied by others to single and multiple wind turbine models, eg. Troldberg et al [90][91][92], and in particular the wind farm simulations of Churchfield et al [22]; these are covered in section 6.2 below.

Lastly there is actuator surface method, an extension of the actuator line concept by Shen et al for for horizontal axis turbines [78] and vertical axis turbines [79]. Rather than representing the aerofoil cross-section as one point on a line, the actuator surface method spreads the force over a notional surface representing the blade aerofoil. Thus the body force exerted on the aerofoil cross-section becomes

$$\underline{f}_{2D}(\underline{x}) = \frac{1}{2} \rho u_{rel}^2 c \left(C_L \underline{e}_L + C_D \underline{e}_D\right) F_{dist}(\underline{x}) \tag{42}$$

Where $F_{dist}(\underline{x})$ is the distribution of pressure force along the blade chord, which is calculated from derived empirical formulae. When compared with actuator line techniques [79], RANS simulations found improvements in the recreation of tip vortices, and the velocity field was more realistic than that produced by actuator line techniques (see Figure 12).

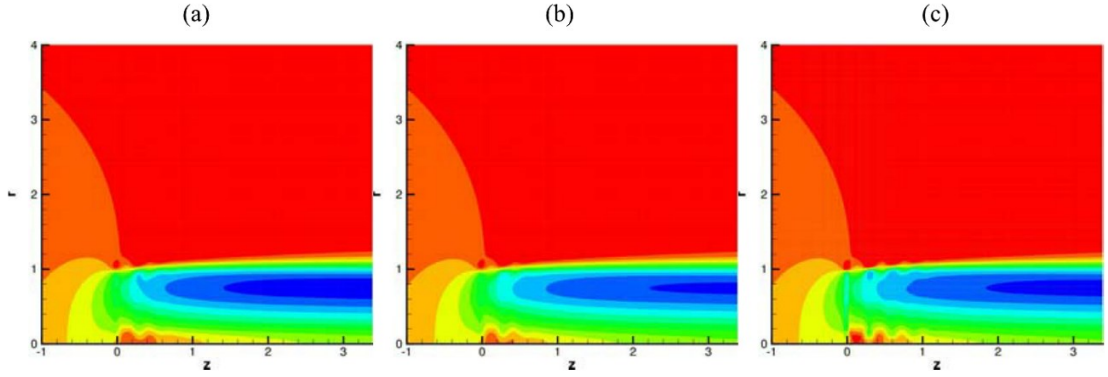

Figure 12. Comparison from RANS simulations in Shen et al [78]: (a) the actuator line method, (b) the actuator surface method, and (c) the actuator surface method with fine mesh.

5.3 Direct representation

Direct, or discrete, representation of single wind turbines for full wake simulation is rare, due to the prohibitive computational cost, and so unheard of for wind farms. However, given the dramatic increase in processing power in recent years, this may not always be the case. Wußow et al [98] used large-eddy simulation to model the turbulent flow behind full-scale turbine, with the rotation rate of the blades set by the incoming freestream wind speed. A three-dimensional domain of 4 million finite volume cells extended from one rotor diameter upwind to 3 diameters downwind, as shown in Figure 13.

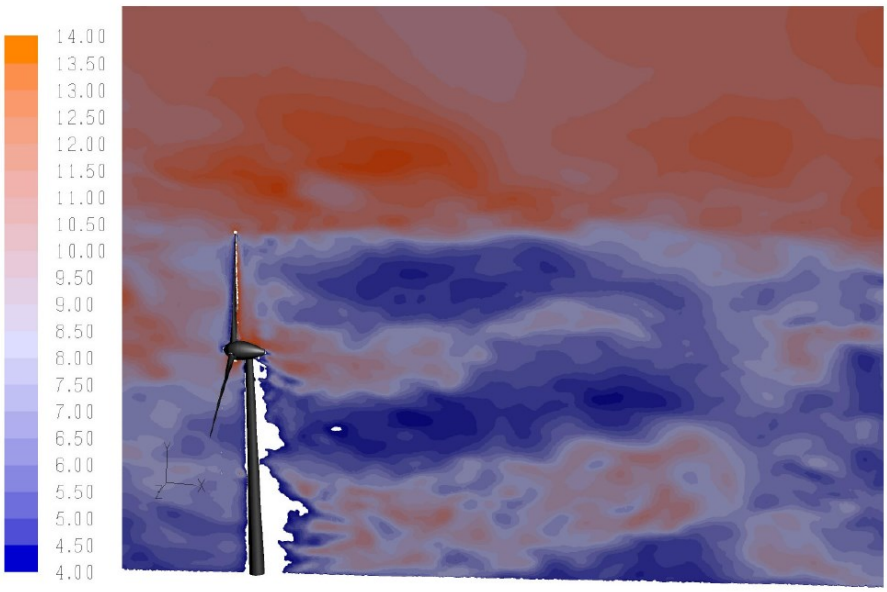

Figure 13. Velocity magnitude in the wake of a discrete turbine simulation (Wußow et al [98]).

Significant wake meandering was a key feature of the wakes produced over the 5 minutes of simulation time, and reasonable agreement was found with measured hub-height velocity data from two diameters downwind; however, the authors noted that the fixed pitch and rotor speed of the model was not a realistic representation of the behaviour of a turbine in turbulent wind conditions – previously, the aerodynamics calculations necessary for more dynamic behaviour were ruled out due to their prohibitive computational complexity.

6 Wind turbine simulations

This section describes main parts of this section describe wind turbine and wind farm models using the two main approaches of modelling turbulent flow, first addressing the Reynolds-Averaged Navier-Stokes (RANS) models and then Large Eddy Simulation (LES).

6.1 RANS models

RANS' computationally inexpensive approach is an attractive prospect for far-wake simulation, and consequently modelling of wind farms. However, reviews by Sanderse [73] and Sumner [86] have found that the $k-\varepsilon$ and $k-\omega$ turbulence models tend to create excess diffusion in the wind turbine wakes, due to the limited applicability of the Boussinesq hypothesis.

In order to reduce the eddy viscosity in the near wake, the approach taken by El Kasmi and Masson [46] was to add a turbulent energy dissipation term to the momentum equation, and apply it around the rotor to limit the turbulent kinetic energy (TKE), and so turbulent eddy viscosity, in order to improve wake predictions. This validity of this approach was confirmed by Cabezón et al [14], who compared RANS simulations of single turbine wakes using the standard $k-\varepsilon$ model with those using the El Kasmi and Masson additions; again the technique was shown to improve the near-wake

turbulence and temper the excessive wake diffusion. Similar analysis using a $k-\omega$ turbulence closure scheme [70], has shown good agreement with Nibe wake data when incorporating the El Kasmi and Masson TKE limiting. A second technique, based on realisability constraints on the Reynolds stress and Schwarz inequality [80] was also shown to perform well. A number of variants of the $k-\varepsilon$ model and a Reynolds Stress Model (RSM) were tested against measurements from a 330 kW wind turbine [15] with the result that the standard $k-\varepsilon$ model tended to underestimate the wake deficit, but that the RSM model and specially tuned variants of the $k-\varepsilon$ model performed better. However, the performance of these depended strongly on the tuning of free parameters in the turbulence models. A whole wind farm in complex terrain was simulated with both analytical wake models and $k-\varepsilon$ RANS models [60], where it became apparent that neither method performed better than others but that all showed considerable variation of prediction error for the different turbines in the farm.

However, as these explicit alterations to the TKE are non-physical, and exist primarily to combat the overestimation of μ_t, it has been questioned whether El Kasmi and Masson's method is applicable to multiple turbine wakes [71]. In their turbine array simulations, Ammara et al [3] did not include explicit turbulence source terms at the turbines, but nonetheless showed reasonable agreement with experimental data from the MOD-2 test wind turbine array at Goldendale.

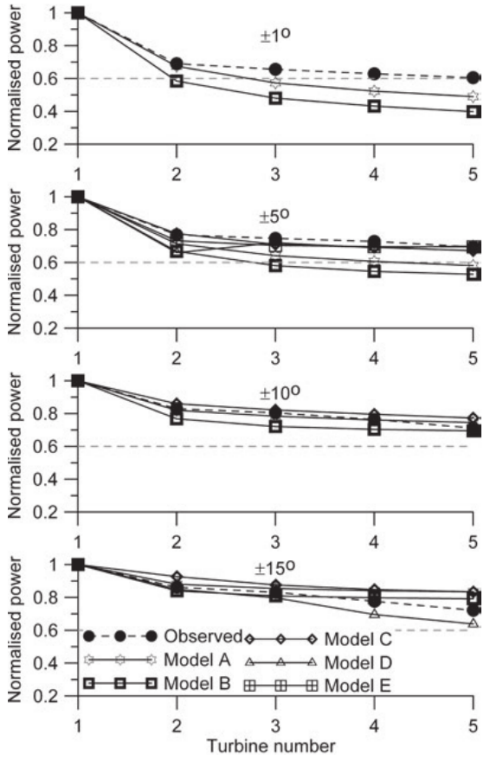

Figure 14. Comparison of models and measurements from Horns Rev for wind direction 270°, showing the power deficits on down wind turbines due to wake effects, at a hub-height freestream wind speed of approximately 8 m/s. The width of the wind direction measurement bins increases from top to bottom. Courtesy of Barthelmie et al [8].

Barthelmie et al [8] carried out a comparison of wind farm models with experimental data from the Horns Rev wind farm, to examine their ability to predict power losses due to wake effects. As shown in Figure 14, they found that models which used $k-\varepsilon$ turbulence closure schemes, such as WAKEFARM (based upon UPMWAKE), CENER and NTUA tended to over predicted wake losses, particularly for narrow wind direction measurement bins.

6.2 LES models

6.2.1 Single turbines

As LES require significantly greater computational resources than RANS methods, its introduction into wind turbine and wind farm modelling has only recently been practicable due to recent advances in affordable computer power. As large-scale turbulence is resolved explicitly, it potentially affords greater accuracy than RANS models, where both small and large scale turbulence are not.

An early important study of the application of LES to modelling wind turbines by Jiminez et al [42] placed a simple thrust actuator disc within cuboid domain, as shown in Figure 15. A dynamic Smagorinsky model (Germano et al [38]) was used to compute C_s , so that it became a function of space and time.

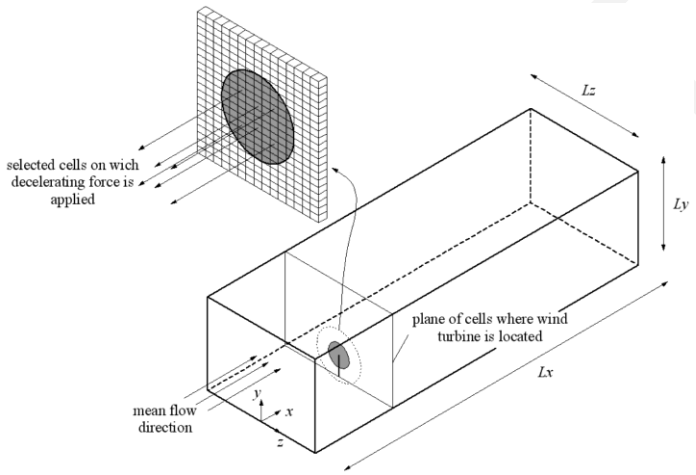

Figure 15. Computational domain used in simulations by Jimenez [42]. The dimensions of the domain are 34.9D x 5.6D x 10.7D. Log law of wall was applied to the rough bottom surface.

The axial force exerted by the disc on the flow was specified as

(43) $$f_x = -C_T \frac{1}{2} A u_0$$

Where C_T is the specified thrust co-efficient, A the cross-sectional area of the rotor disc, and u_0 the freestream flow speed upwind. Simulation results were compared with measurement data from Sexbierum wind farm, a sample of which are shown in Figure 16. This work was later extended for spectral analysis and further comparison with measurements wind farms [43].

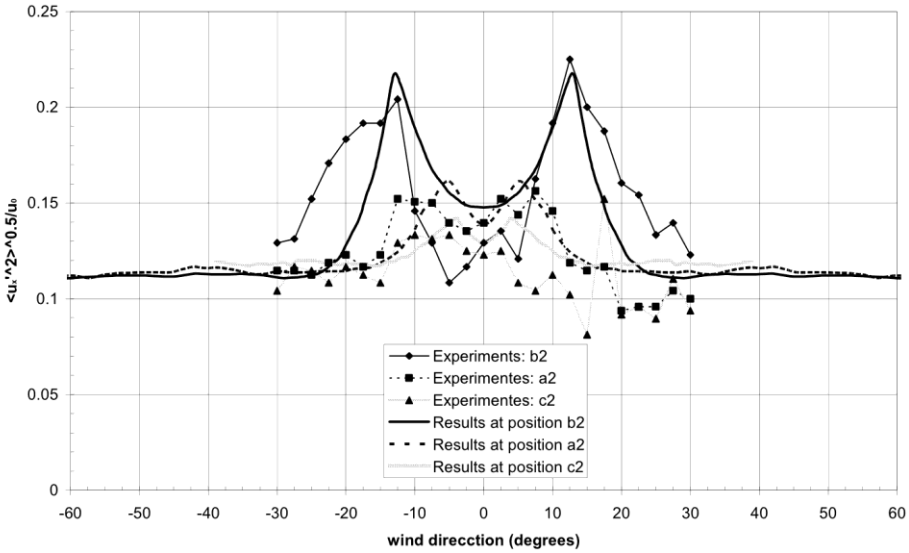

Figure 16. Turbulence intensity as it varies with flow direction at a downstream distance of 2.5D, courtesy of Jimenez [42].

Despite the simplicity of the turbine model, LES was shown to have good qualitative agreement with experimental measurements of turbulence, demonstrating that it could be a viable technique for wind turbine wake analysis. Similar wind tunnel experiments and LES wind tunnel simulations to test the effect of including wake rotation in the actuator disk model also showed very good quantitative agreement with the experimental data, as long as the wake rotation was included in the model [97].

A more sophisticated model was used by Troldborg et al [92], who took the actuator line technique developed by Sørensen and Shen [82] and coupled it with the Ellipsys3D flow solver [59][83], with LES modelling using mixed-scale model. Simulations ran a cuboid wind-tunnel type structure; the fully-developed downstream wakes are shown in Figure 17.

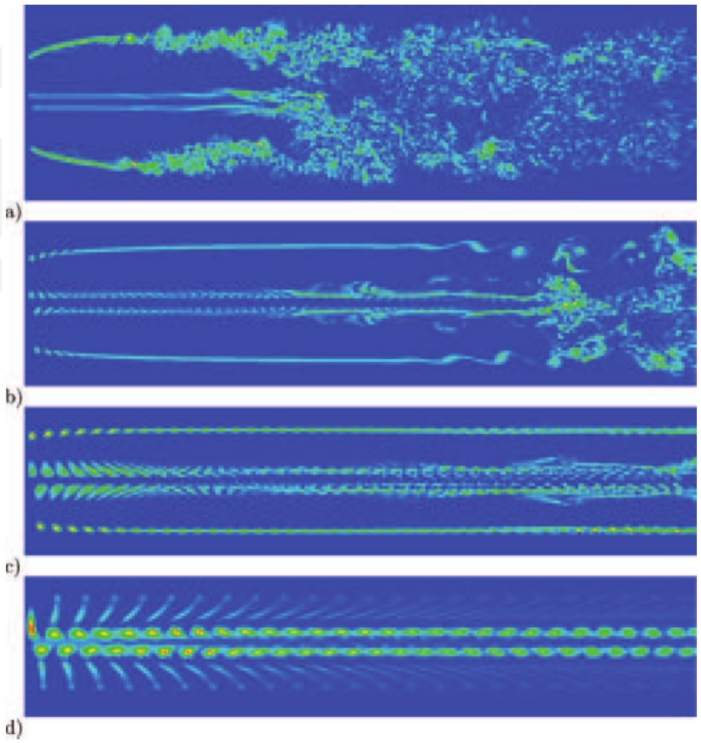

Figure 17. Vorticity plot of downstream wake for Troldberg [91] for upstream flow speeds of a) u0=6 m/s, b) u0=10m/s, c) u0=14 m/s and d) u0=22 m/s.

On a larger scale, Creech et al [27] extended an actuator volume turbine model of wind and tidal turbine simulations using LES [26], to develop a hybrid blade-element / CFD model to simulate a single turbine in a large domain with irregular terrain at Myres Hill, using a finite-element CFD with LES [68] for resolving the flow. Rather than having any notion of individual blades as in the actuator line method above, the forces exerted by the blades on the flow varied radially, but were azimuthally smoothed in concentric rings from the hub to the tip. Turbulence was generated in two defined sub-volumes: the main blade section, and the tip section as delineated in Figure 18.

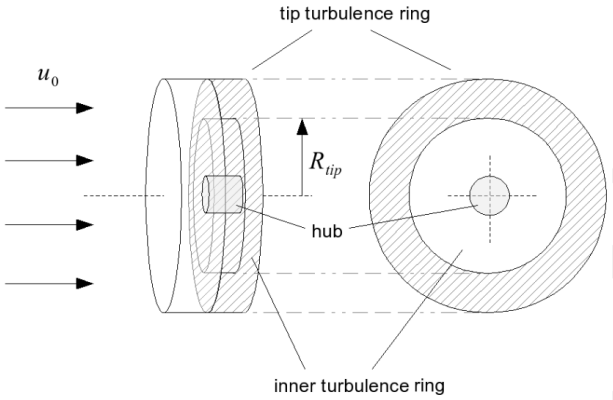

Figure 18. The tip turbulence rings in the actuator volume model by Creech et al [27].

LIDAR measurements were taken from the physical site for comparison; good qualitative agreement was found in comparative wake decay rates, as seen in Figure 19.

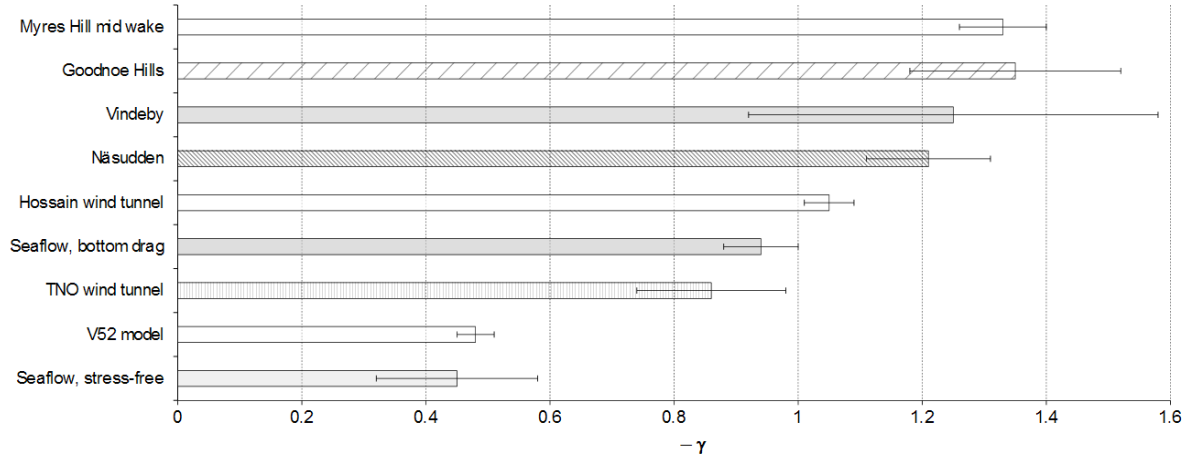

Figure 19. Decay rate of turbine wakes from both simulation and previous wind tunnel and experimental data, Creech et al [27].

6.2.2 Wind farms

Due to its virtue of handling large-scale turbulence explicitly, large eddy simulation has recently been used to study the fluid dynamics of wind farms. In their paper, Calaf et al [17] compared LES models to study the effects of large wind farms on the atmospheric boundary layer (see Figure 20). Here, they use thrust (or "drag") discs to model the wind turbines in an array, to develop the idea of a wind turbine array boundary layer (WTABL), conceptually dividing the flow into two layers: one below and one above the turbines' hub height. This allowed them to examine the downward transport of kinetic energy towards the turbines, to parameterise the effective roughness generated by the action of the turbines on the upper layer, in a similar manner to that of Lettau [54].

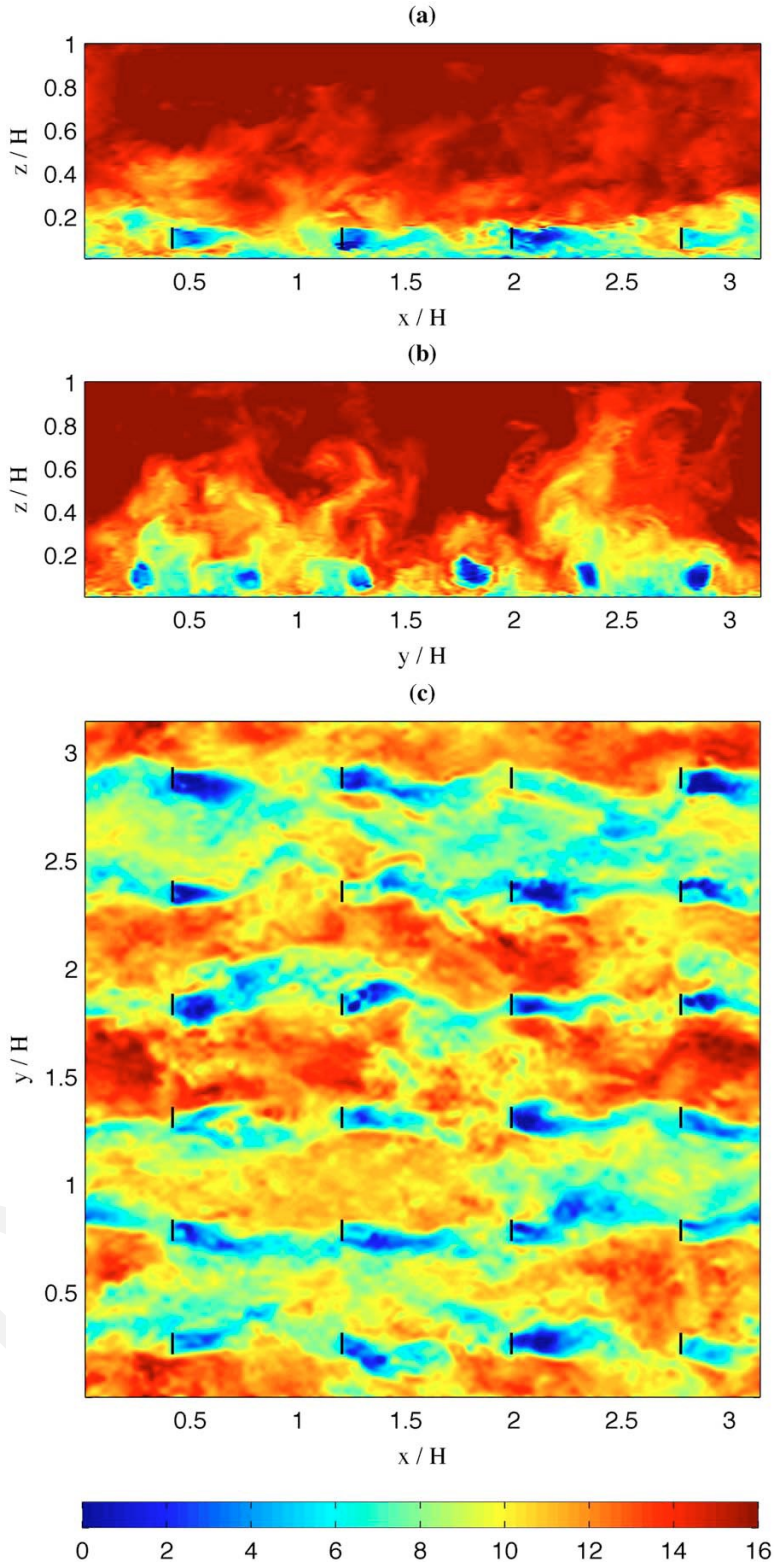

Figure 20. Colour plot of velocity from LES of a fully developed WTABL case, with black lines representing the modelled turbines: a) on a vertical plane, from the side; b) a vertical cross-stream plot 1D downstream of a turbine row; c) a horizontal plot at hub height. From Calaf et al [17].

Lu and Porté-Agel [56] developed a model based upon Sørensen and Shen's actuator line technique [82], with rotor RPM parameterised by freestream wind speed. Rather than model the entire wind farm explicitly, Lu et al applied periodic boundary conditions horizontally to the domain in Figure 21, so that in effect a wind farm of infinite extent could be simulated. The domain was extended

downstream by distances of 5D and 8D, at the expense of not modelling the development of the flow from the unperturbed free stream to the developed flow within the farm.

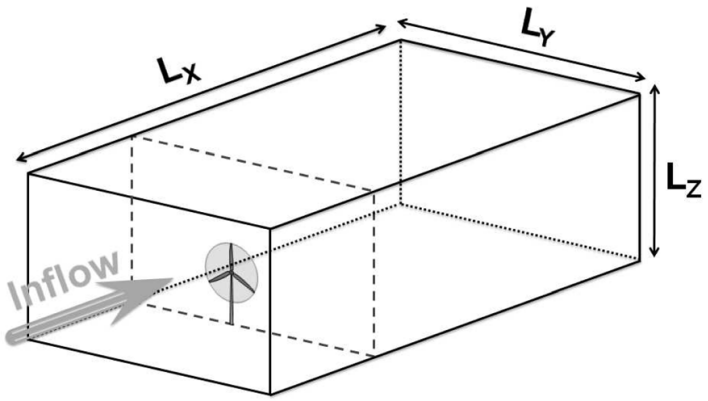

Figure 21. Schematic of computational domain in Lu and Porté-Agel [56].

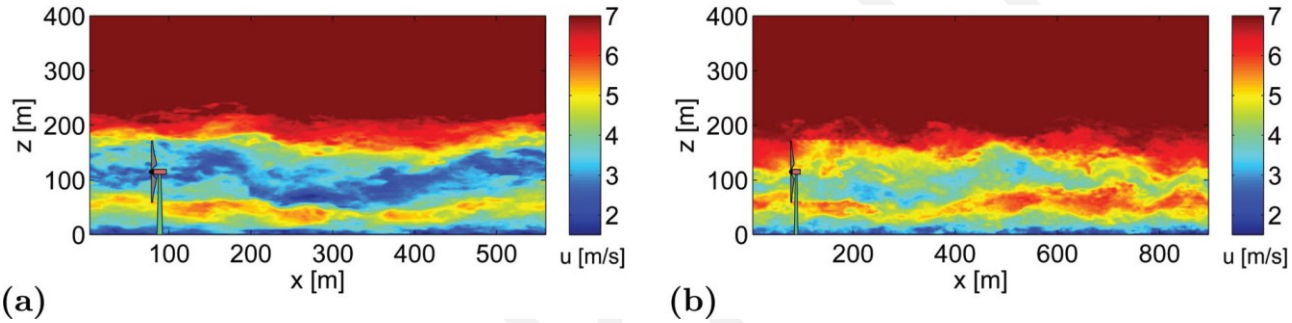

Figure 22. Vertical slices through x-component of velocity field for a) 5D and b) 8D cases, courtesy of Lu and Porté-Agel [56].

In their findings, they report that whilst closer spacing of turbines results in greater power extraction, it also increases the atmospheric boundary layer height, and overall turbulence intensity. In 2011, Porté-Agel et al [69] compared three turbine models in the simulation with wake measurements from an actual wind farm: an actuator disc model with no rotation (ADM-NR), actuator disc with rotation (ADM-R), and an actuator line model (ALM). The latter two produced good agreements with SODAR data, as well as having higher turbulence intensity measurements when compared to ADM-NR. ADM-NR consistently under-predicted wake deficits and consequently over-predicted power outputs of downwind turbines. The ADM-R and ALM techniques produced power reductions within 2% of actual SCADA data, suggesting that wake rotation and associated turbulence has a key role in wake diffusion.

7 Discussion and Conclusions

7.1 Comparison of CFD methods

This short overview over the various methods used to model wind turbine wakes there are many approaches being used where all have their respective strengths and weaknesses.

The models based on the vorticity are attractive because they reflect the fact that the action of the turbine blades is through the bound vortex induced by the aerofoil shape of the blade and because they easily describe the transport of vortex features shed by the turbine blades. Their weaknesses, however, are that they cannot easily incorporate solid boundaries, especially in complex geometries,

and that they become computationally very expensive and unstable as the complexity of the system increases to allow for free wake development. This is largely due to the need for either solving three Poisson equations – rather than one as for the momentum-pressure formulation – or for integrating Biot-Savart's law over a large domain for each vortex. Considering that this is likely to be a key element for full wind farm modelling, this will be a considerable challenge to a widespread adoption of this approach.

Models based on the momentum and pressure formulation of the Navier-Stokes equations are, in a way, more straight-forward as the momentum equation is based on the local momentum balance and only the pressure has to be solved through a single Poisson equation, for which a large number of well-tested solvers exist. However, since the forces on the turbine blades and their reactions in the fluid are due to surface forces, their direct representation for a wind farm would require a model resolution well beyond any imaginable computing resource and a time step so small to make any such simulation take an extremely long time. This has led to the various approaches of replacing the actual surface forces by other representations, such as the induced velocities from the vorticity of the aerofoils, or by approximating the surface forces by volume forces estimated from actuator disk theory or boundary element momentum theory approaches.

Once the forces are parameterised, their effect on the flow through the momentum equation is calculated on either a structured or unstructured mesh or grid. While a structured mesh is computationally more effective, it is less able to optimise the resolution to spatially very diverse geometries and flow fields. Unstructured meshes, on the other hand can concentrate model resolution in spaces where it is needed, either through careful design of a fixed unstructured mesh or through an adaptive mesh which adjusts to the local flow field. While this is, in principle, a very powerful technique it requires careful control over the mesh adaptation steps.

The two main contenders in choice of CFD modelling choices are Reynolds-Averaged Navier-Stokes (RANS) and Large Eddy Simulation (LES). RANS has long been established as a reliable and stable tool for many engineering situations and, for that reason, is available through a large number of commercial packages. Since RANS solves the equations of motion for the mean flow and a bulk turbulence intensity it cannot explicitly model the actual turbulent velocities and therefore tends to result in smoothed flow solutions, irrespective of whether traditional RANS or unsteady RANS (URANS) is used. As a consequence, the results should only ever be interpreted as averaged approximations of the true case. That said, for the same reason it is computationally relatively cheap and can easily be used on standard desktop computers. LES solves the actual velocities from the Navier-Stokes equations at the resolved scales and only parameterises the effect of small-scale effects through a suitably calculated eddy viscosity. This suggests that LES should give a closer representation of the flow but only if all relevant scales are sufficiently resolved by the mesh or grid, and it is not always clear what is 'sufficient'. It can also easily be seen that the computational costs of LES are much higher than those of RANS, and the concept of adaptive meshing becomes very attractive. However, care must be taken that adaptivity does not allow apparently peripheral flow to be excessively smoothed. For example, if the resolution is very high near the turbines but very coarse in a relatively featureless upstream part of the domain, the coarse resolution far upstream will eliminate most freestream turbulence which the model cannot re-inject into that fluid once it approaches the turbines.

One option to reduce the computational cost is to replace the region close to solid boundaries, such as complex terrain, by a function which simulates the effect from surface drag onto the main fluid through a wall function, e.g. Bou-Zeid et al [16] or Anderson et al [4]. However, to provide an adequate wall function for a complex surface such as the land surrounding a wind farm, is

problematic and the benefits of using LES are potentially negated by inadequate representation of the effects of the surface on the wind shear and turbulence characteristics.

An attempt to combine the strengths of LES and the economy of RANS led to a number of hybrid RANS/LES approaches such as Detached Eddy Simulation (DES) [85][88], or a refinement of it, delayed DES (DDES) [84]. A similar hybrid approach was applied to a wind farm by Bechmann and Sørensen [10]. As the area of interest for wind farm modelling is the free flow in the wakes, the fluid away from surfaces is modelled through LES but in near-wall regions, the model switches to RANS. Compared to a typical domain depth of several hundreds of metres or even a few km, the level of the switch from LES to RANS at around 6 m is very small, and the RANS surface model can be regarded as an advanced wall model. Computationally, this approach is more marginally more expensive than using a wall function but provides a more rational way of incorporating the forcing from the surface. As this approach is not yet fully explored, it is too early to judge its performance yet but it has demonstrated that it is worth developing further.

7.2 Conclusions

After this survey, it would be tempting to ask 'so which one is the best?'. The answer would have to depend on the purpose of the wind farm modelling. Would it be to obtain an estimate of an annual electricity production potential for a wind farm with a given wind rose? Would it be optimise the wind farm layout? Would it be to investigate the blade loading for a particular rotor within a wind farm? Would it be for a fundamental fluid dynamics phenomenon or fluid-structure interaction? Each of these would probably be best investigated with a different approach.

To illustrate the case, let us return to the observed relative performance of downstream turbines in Lillgrund wind farm shown in Figure 2 as a mean relative power output against wind direction. That figure suggests that it should be sufficient to use a relatively cheap model and run it for a fairly large number of wind directions, possibly even seeking steady-state solutions, in which case RANS and simple turbine models might be the best. However, if we consider the actual measurements used to generate the mean values in Figure 2, a different picture emerges. Figure 23 shows the relative power of the second turbine only over a 20-degree sector where each point represents a valid SCADA measurement from a three-year measurement period at 10 minutes interval. Superimposed on this are the mean and one standard deviation either side of the mean. The dots clearly show that the wind farm performance shows strong fluctuations at each notional wind direction, where it is not known whether the variation arises through inherent turbulence of the wake or through wake meandering caused by upstream turbulence and wind speed changes. In terms of most accurate modelling of the wind farm, a model should reproduce this variability if given appropriate turbulence inlet conditions; this would only be possible with a high-resolution LES model. Similarly, evaluating the forces on wind turbines with a view to investigate reliability or performance, it is important to resolve turbulence appropriately [44], and LES would be required for this. In terms of annual or weekly electricity output, the ability to reproduce the red lines would be sufficient. In that case, RANS might be most appropriate as it models the mean flow and is computationally cheap enough to run many simulations at different wind directions.

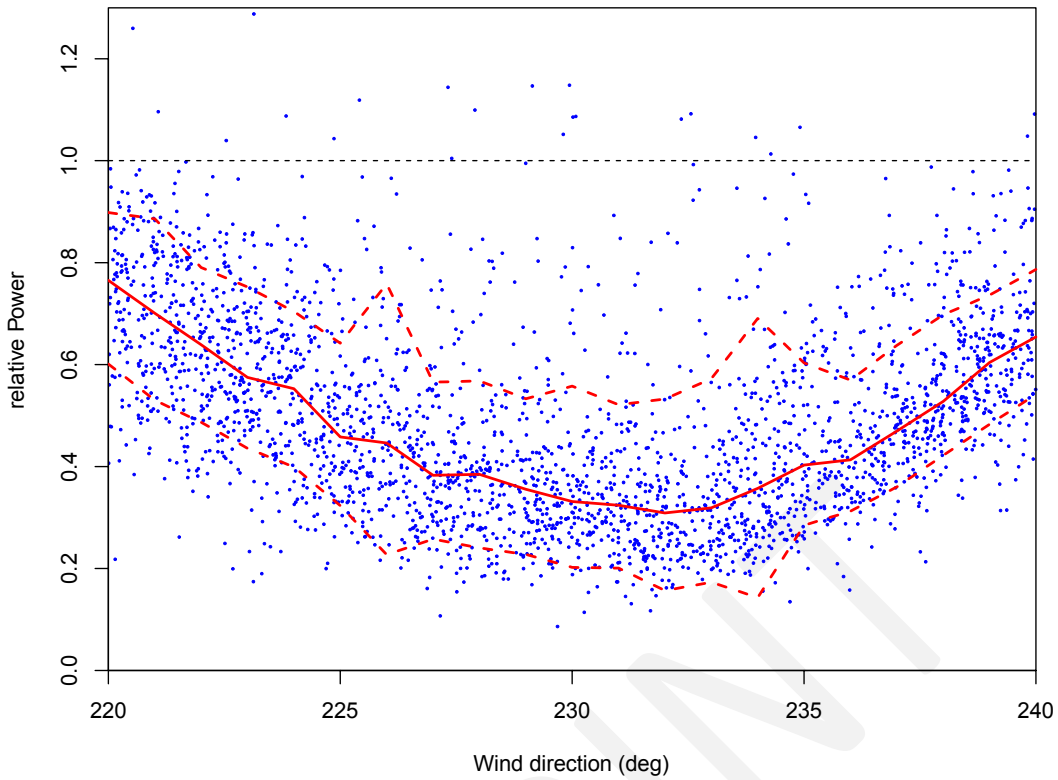

Figure 23. Scatter plot of the relative power output of the 2nd-row turbine over front turbine when, when freestream is between the cut-in and rated wind speed, against wind direction. Measurements (dots), mean (red solid line), standard deviation (red dashed lines). Data source: Vattenfall for Lillgrund wind farm, turbines C07 and C08.

8 References

[1] M.S. Adaramola and P.Å. Krogstad. Experimental investigation of wake effects on wind turbine performance. *Renewable Energy*, 36(8):2078–2086, 2011.

[2] J.F. Ainslie. Calculating the flowfield in the wake of wind turbines. *Journal of Wind Engineering and Industrial Aerodynamics*, 27:213–224, 1988.

[3] I. Ammara, C. Leclerc and C. Masson. A Viscous Three-Dimensional Differential/Actuator-Disk Method for the Aerodynamic Analysis of Wind Farms. *J. Sol. Energy Eng*, 124(4):345–346, 2002.

[4] W.C. Anderson, S. Basu, W.L. Letchford. Comparison of dynamic subgrid-scale models for simulations of neutrally buoyant shear-driven atmospheric boundary layer flows. *Environmental Fluid Mechanics*, 7:195 – 215, 2007.

[5] ANSYS, Inc. ANSYS CFX Introduction. *Technical manual*, 2010.

[6] A.A. Afjeh and T.G. Keith. A simplified free wake method for horizontal-axis wind turbine performance prediction. *Trans ASME; J Fluids Eng*,108:303–9, 1986.

[7] R.J. Barthelmie, L. Folkerts, G. C. Larsen, K. Rados, S. C. Pryor, S. T. Frandsen, B. Lange and G. Schepers. Comparison of Wake Model Simulations with Offshore Wind Turbine Wake Profiles Measured by Sodar. *Journal of Atmospheric and Oceanic Technology* 23:888–901, 2006.

[8] R. J. Barthelmie, K. Hansen, S. T. Frandsen, O. Rathmann, J. G. Schepers, W. Schlez, J. Phillips, K. Rados, A. Zervos, E. S. Politis, and P. K. Chaviaropoulos. Modelling and measuring flow and wind turbine wakes in large wind farms offshore. *Wind Energy*, 12:431–444, 2009.

[9] R.J. Barthelmie, S.C. Pryor, S.T. Frandsen, K.S. Hansen, J.G. Schepers, K. Rados,WSchlez, A. Neubert, L.E. Jensen, and S. Neckelmann. Quantifying the impact of wind turbine wakes on power output at offshore wind farms. *J. Atmos Ocean Tech*., 27(8):1302 – 1317, 2010.

[10] A. Bechmann and N.N. Sørensen. Hybrid RANS/LES applied to complex terrain. *Wind Energy*, 14: 225–237, 2011.

[11] P. Beaucage, M. Brower, N. Robinson and C. Alonge. Overview of six commercial and research wake models for large offshore wind farms. *Proceedings EWEA 2012,* Copenhagen, April 2012.

[12] F. Bertagnolio, N. Sørensen, J. Johansen and P. Fugslang. *Wind turbine airfoil catalogue*. Technical report. Risø National Laboratory, Risø-R-1280(EN), 2001.
[13] T. Burton, D. Sharpe, N. Jenkins and E. Bossanyi. *Wind Energy Handbook*. Wiley, 2006.
[14] D. Cabezón, J. Sanz, I. Martí and A. Crespo. CFD Modelling of the Interaction Between the Surface Boundary Layer and Rotor Wake: Comparison of Results Obtained with Different Turbulence Models and Mesh Strategies. *Proceedings of EWEC 2009*, Marseilles, 2009.
[15] D. Cabezon, E. Migoya, and A. Crespo. Comparison of turbulence models for the computational fluid dynamics simulation of wind turbine wakes in the atmospheric boundary layer. *Wind Energy*, 14(7):909–921, 2011.
[16] E. Bou-Zeid, C. Meneveau, and M.B. Parlange. A scale-dependent Lagrangian dynamic model for large eddy simulation of complex turbulent flows. *Physics of fluids,* 17, 2005.
[17] Marc Calaf, Charles Meneveau, and Johan Meyers. Large eddy simulation study of fully developed wind-turbine array boundary layers. *Physics of Fluids*, 22(1), 2010.
[18] D.M. Canu, C. Solidoro, and G. Umgiesser. Modelling the responses of the Lagoon of Venice ecosystem to variations in physical forcings. *Ecological Modelling*, 170:265–289, 2003.
[19] L.P. Chamorro and Fernando Porte-Agel. A wind-tunnel investigation of wind-turbine wakes: Boundary-layer turbulence effects. *Boundary-Layer Meteorology*, 132(1):129–149, 2009.
[20] L.P. Chamorro and Fernando Porte-Agel. Turbulent flow inside and above a wind farm: A wind-tunnel study. *Energies*, 4(11):1916–1936, 2011.
[21] T.J. Chung. *Finite Element Analysis in Fluid Dynamics*. McGraw-Hill, 1978.
[22] M.J. Churchfield, S. Lee, P.J. Moriarty, L.A. Martínez, S. Leonardi, G. Vijayakumar and J.G. Brasseur. A Large-Eddy Simulation of Wind-Plant Aerodynamics. *50th AIAA Aerospace Sciences Meeting including the New Horizons Forum and Aerospace Exposition*, 2012.
[23] F.N. Coton and T. Wang. The prediction of horizontal axis wind turbine performance in yawed flow using an unsteady prescribed wake model. *Proceedings of the Institution of Mechanical Engineers, Part A. J Power Energy*, 213:33–43, 1999.
[24] F.N. Coton, T. Wang, and R.A.M. Galbraith. An examination of key aerodynamic modelling issues raised by the NREL blind comparison. *Wind Energy*, 5:199–212, 2002.
[25] G.H. Cottet and P.D. Koumoutsako. *Vortex methods: theory and practice*. Cambridge University Press, New York, 2000.
[26] A.C.W. Creech. *A three-dimensional numerical model of a horizontal axis, energy extracting turbine*. PhD thesis, Heriot-Watt University, 2009. (Available from: www.ros.hw.ac.uk).
[27] A.C.W. Creech, W.-G. Früh, and P. Clive. Actuator volumes and hr-adaptive methods for 3D simulation of wind turbine wakes and performance. *Wind Energy*, 2011.
[28] A. Crespo, F. Manuel, D. Moreno, E. Fraga and J. Hernández, `Numerical analysis of wind turbine wakes', *Proc. Delphi Workshop on Wind Energy Applications*, Delphi, pp. 15–25, 1985.
[29] A. Crespo and J. Hernández. Numerical modelling of the flow field in a wind turbine wake. *Proc. 3rd Joint ASCE/ASME Mechanics Conf., Forum on Turbulent Flows*, La Jolla, CA, pp. 121–127, 1989.
[30] A. Crespo, J. Hernandez and S. Frandsen. Survey of modelling methods for wind turbine wakes and wind farms. *Wind Energy*, 2:1–24, 1999.
[31] Jan-Åke Dahlberg. *Assessment of the Lillgrund Windfarm: Power Performance, Wake Effects*. Technical report. Vattenfall AB, September 2009.
[32] J.Å. Dahlberg and D. Medici. Potential improvement of wind turbine array efficiency by active wake control (AWC). *Proc. European Wind Energy Conference and Exhibition*, Madrid, Spain, 16–19 June; 2003.
[33] J.P. Van Doormal and G.D. Raithby. Enhancement of SIMPLE method for predicting incompressible fluid flows. *J. Numerical Heat Transfer*, 7:147–163, 1984.
[34] P. R. Ebert and D. H. Wood. The near wake of a model horizontal-axis wind turbine – II. General features of the three-dimensional flowfield. Ren. Energy, 18:513–534, 1999.
[35] J.H. Ferziger and M. Perić. *Computational Methods for Fluid Dynamics*. 3rd edition. Springer-Verlag, 2002.
[36] C.A.J Fletcher. *Computational Techniques for Fluid Dynamics*, volume 2. Springer Series in Computational Physics, 1991.
[37] S. Frandsen, R. Barthelmie, S. Pryor, O. Rathmann, S. Larsen, and J. Højstrup. Analytical modelling of wind speed deficit in large offshore wind farms. *Wind Energy,* 9:39–53, 2006.

[38] M. Germano, U. Piomelli, P. Moin and W.H. Cabot. A Dynamic Subgrid-Scale Eddy Viscosity Model. *Proceedings of Summer Workshop*, Center of Turbulence Research, Stanford University, 1990.
[39] M.O.L. Hansen, J.N. Sørensen and W.Z. Shen. Vorticity–velocity formulation of the 3D Navier–Stokes equations in cylindrical co-ordinates. *Int. J. Numer. Meth. Fluid*, 41:29–45, 2003.
[40] M.O.L. Hansen. *Vorticity-velocity formulation of the Navier-stokes equations for aerodynamic flows*. PhD thesis, Department of Fluid Mechanics, Technical University of Denmark, 1994.
[41] N.O. Jensen. *A note on wind generator interaction*. Technical Report. Risø National Laboratory, Roskilde, Denmark, 1983.
[42] A. Jimenez, A. Crespo, E. Migoya, and J. Garcia. Advances in large-eddy simulation of a wind turbine wake. *Journal of Physics Conference Series*, 75:12041–12041, 2007.
[43] A. Jimenez, A. Crespo, E. Migoya, and J. Garcia. Large-eddy simulation of spectral coherence in a wind turbine wake. *Environmental Research Letters*, 3(1), 2008.
[44] Angel Jimenez, Emilio Migoya, Millan Esteban, David Gimenez, Javier Garcia, and Antonio Crespo. Influence of topography and wakes on wind turbulence: measurements and interpretation of results. *Wind Energy*, 14(7):895–908, 2011.
[45] J. Jonkman, S. Butterfield, W. Musial and G. Scott,. Definition of a 5-MW Reference Wind Turbine for Offshore System Development. Technical Report, National Renewable Energy Laboratory, Rept. NREL/TP-500-38060, Golden, CO, Jan. 2009.
[46] A. El Kasmi and C. Masson. An extended $k-\varepsilon$ model for turbulent flow through horizontal axis wind turbines. *J. of Wind Engineering*, 96:103–122, 2008.
[47] I. Katic, J. Højstrup, and N.O. Jensen. A simple model for cluster efficiency. *Proceedings from the European Wind Energy Conference*, Rome, Italy, 1986.
[48] G.C. Larsen, H.A. Madsen, H.A. Thomson and T. J. Larsen. Wake meandering – a pragmatic approach. *Wind Energy*, 11:377–395, 2008.
[49] G.C. Larsen and A. Crespo. Wind turbine wakes for wind energy. *Wind Energy*, 14(7):797–798, 2011.
[50] G.C. Larsen, Helge Aa Madsen, Kenneth Thomsen, and Torben J. Larsen. Wake meandering: A pragmatic approach. *Wind Energy*, 11(4):377–395, 2008.
[51] J.W. Larsen, S.R.K. Nielsen and S. Krenk. Dynamic stall model for wind turbine aerofoils. *Journal of Fluids and Structures*, 23:959–982, 2007.
[52] B.E. Launder and D.B. Spalding. The numerical computation of turbulent flows. *Computer Methods in Applied Mechanics and Engineering*, 3:269–289, 1974
[53] S. Legrand, V. Legat, and E. Deleersnijder. Delaunay mesh generation for an unstructured-grid ocean general circulation model. *Ocean Modelling*, 2:17–28, 2000.
[54] H. Lettau. Note on aerodynamic roughness-parameter estimation on the basis of roughness-element description. *J. Appl. Meteorology*, 8:828, 1969.
[55] Y. Li and S.M. Çalişal. A Discrete Vortex Method for Simulating a Stand-Alone Tidal-Current Turbine: Modeling and Validation. *J. Offshore Mech. Arct. Eng*., 132, 2010.
[56] Hao Lu and Fernando Porte-Agel. Large-eddy simulation of a very large wind farm in a stable atmospheric boundary layer. *Physics of Fluids*, 23(6), 2011.
[57] C. Masson, A. Smaïli and C. Leclerc. Aerodynamic Analysis of HAWTs Operating in Unsteady Conditions. *Wind Energy*, 4:1–22, 2001.
[58] J. Meyers and C. Meneveau. Large eddy simulations of large wind-turbine arrays in the atmospheric boundary layer. *48th AIAA Aerospace Sciences Meeting*, Orlando, Florida, January 2010.
[59] J.A. Michelsen. *Basis3D – A platform for development of multiblock PDE solvers*. Technical report. Department of Fluid Mechanics, Technical University of Denmark, DTU, 1994.
[60] Emilio Migoya, Antonio Crespo, Javier Garcia, Fermin Moreno, Fernando Manuel, Angel Jimenez, and Alexandre Costa. Comparative study of the behavior of wind-turbines in a wind farm. *Energy*, 32(10):1871–1885, 2007.
[61] R.H. Miller. The aerodynamic and dynamic analysis of horizontal axis wind turbines. *J. Wind Eng Ind Aerodyn*, 15:329–40, 1983.
[62] G. Mosetti, C. Poloni and B. Diviacco. Optimization of wind turbine positioning in large wind farms by means of a genetic algorithm, *Journal of Wind Engineering and Industrial Aerodynamics*, 97:105–116, 1994.
[63] D. Nechaev, J. Schrter, and M. Yaremchuk. A diagnostic stabilized finite-element ocean circulation model. *Ocean Modelling*, 5 (1):37–63, 2003.

[64] S. Øye. A simple vortex model. *Proceedings of the Third IEA Symposium on the Aerodynamics of Wind Turbines*, ETSU, Harwell, pp. 4.1–5.15, 1990.
[65] C.C. Pain, M.D. Piggot, A.J.H. Goddard, F. Fang, G.J. Gorman, D.P. Marshall, M.D. Eaton, P.W. Power, and C.R.E. de Oliveira. Three-dimensional unstructured mesh ocean modelling. *Ocean Modelling*, 10:533, 2005.
[66] S.V. Patankar and D.B. Spalding. A calculation procedure for heat, mass and momentum transfer in three-dimensional parabolic flows. *International Journal of Heat Mass Transfer*, 15:1787–1806, 1972.
[67] S.V. Patankar. *Numerical heat transfer and fluid flow*. McGraw-Hill, 1980.
[68] M.D. Piggott, C.C Pain, G.J. Gorman, P.W. Power, A.J.H. Goddard. h, r, and hr adaptivity with applications in numerical ocean modelling. *Ocean Modelling*, 10: 95–113, 2004.
[69] Fernando Porte-Agel, Yu-Ting Wu, Hao Lu, and Robert J. Conzemius. Large-eddy simulation of atmospheric boundary layer flow through wind turbines and wind farms. *Journal of Wind Engineering and Industrial Aerodynamics*, 99(4):154–168, 2011.
[70] J. Prospathopoulos, E. Politis, K. Rados, and P. Chaviaropoulos. Enhanced CFD Modelling of Wind Turbine Wakes. *Extended Abstracts for Euromech Colloquium 508 on Wind Turbine Wakes*m European Mechanics Society, Madrid, 2009.
[71] P.E. Réthore. *Wind Turbine Wake in Atmospheric Turbulence*. PhD thesis, Aalborg University, 2009.
[72] B. Sanderse. *Aerodynamics of wind turbine wakes*. Technical report. Energy Research Centre of the Netherlands, 2009.
[73] B. Sanderse, S. P. van der Pijl, and B. Koren. Review of computational fluid dynamics for wind turbine wake aerodynamics. *Wind Energy*, 14(7):799–819, 2011.
[74] J.G. Schepers and S.P. van der Pijl. Improved modelling of wake aerodynamics and assessment of new farm control strategies. *Journal of Physics: Conference Series*, vol. 75, 2007.
[75] S.J. Schreck, N.N. Sørensen and M.C. Robinson. Aerodynamic structures and processes in rotationally augmented flow fields. *Wind Energy*, 10:159–178, 2007.
[76] F.G. Schmitt. About Boussinesq's turbulent viscosity hypothesis: historical remarks and a direct evaluation of its validity. *Comptes Rendus Mécanique*, 335 (9-10): 617-627, 2007.
[77] W.Z. Shen and M.O.L. Hansen. Determination of the angle of attack on rotor blades. *Wind Energy*, 12:91–98, 2009.
[78] W.Z. Shen, J.N. Sørensen and J.H. Zhang. Actuator Surface Model for Wind Turbine Flow Computations. *Proceedings of European Wind Energy Conference*, Milan, 2007.
[79] W.Z. Shen, J.H. Zhang and J.N. Sørensen. The Actuator Surface model: A New Navier-Stokes Based Model for Rotor Computations. *J. Sol. Energy Eng*, 131(1), 2009.
[80] T.-H. Shih, J. Zhu and J.L. Lumley. A new Reynolds stress algebraic equation model. *Comput. Methods Appl. Mech. Engrg*, 125:287–302, 1995.
[81] J.N. Sørensen, W.Z. Shen and X. Munduate. Analysis of wake states by a full-field actuator disc model. *Wind Energy*, 1:73–88 , 1998.
[82] J.N. Sørensen and W.Z. Shen. Numerical modelling of wind turbine wakes. *Journal of Fluids Engineering*, 124:393–399, 2002.
[83] N.N. Sørensen. *General purpose flow solver applied to flow over hills*. PhD Thesis, Risø-R-827(EN), Risø National Laboratory, Roskilde, Denmark, 1995.
[84] N.N. Sørensen. CFD modelling of laminar-turbulent transition for airfoils and rotors using the γ-Re_θ model. *Wind Energy*, 12:715–733, 2009.
[85] P.R. Spalart. Detached-eddy simulation. *Annual Review of Fluid Mechanics*, 41:181–202, 2009.
[86] Jonathon Sumner, Christophe Sibuet Watters, and Christian Masson. CFD in wind energy: The virtual, multiscale wind tunnel. *Energies*, 3(5):989–1013, 2010.
[87] M. Steinbuch, W.W. de Boer, O.H. Bosgra, S.A.W.M. Peters, and J. Ploeg. Optimal control of wind power plants. *Journal of Wind Engineering and Industrial Aerodynamics*, 27: 237–246, 1988.
[88] M. Strelets. Detached eddy simulation of massively separated flows. *AIAA paper*, 2001-879, 2001.
[89] T. Thiringer and A. Petersson. Control of a variable-speed pitch-regulated wind turbine. *Technical Report*, Chalmers University of Technology, 2005.
[90] Niels Troldborg, Gunner C. Larsen, Helge A. Madsen, Kurt S. Hansen, Jens N. Sorensen, and Robert Mikkelsen. Numerical simulations of wake interaction between two wind turbines at various inflow conditions. *Wind Energy*, 14(7):859–876, 2011.

[91] Niels Troldborg, Jens N. Sorensen, and Robert Mikkelsen. Actuator line simulation of wake of wind turbine operating in turbulent inflow - art. no. 012063, volume 75 of *Journal of Physics Conference Series*, pp. 12063–12063. 2007.

[92] Niels Troldborg, Jens N. Sorensen, and Robert Mikkelsen. Numerical simulations of wake characteristics of a wind turbine in uniform inflow. *Wind Energy*, 13(1):86–99, 2010.

[93] L. J. Vermeer, J. N. Sorensen, and A. Crespo. *Wind turbine wake aerodynamics*. Prog. Aerosp. Sci., 39:467–510, 2003.

[94] WAKEBENCH: Benchmarking of Wind Farm Flow Models. Website, URL: http://www.ieawind.org/summary_page_31.html. Retrieved 16th May, 2012.

[95] D. Wilcox. Formulation of the k-w Turbulence Model Revisited. *AIAA Journal*, 46(11):2823–2838, 2008.

[96] C.R. Wilson. *Modelling multiple-material flows on adaptive unstructured meshes*. Ph.D Thesis, Imperial College London, 2009.

[97] Yu-Ting Wu and Fernando Porte-Agel. Large-eddy simulation of wind-turbine wakes: Evaluation of turbine parametrisations. *Boundary-Layer Meteorology*, 138(3):345–366, 2011.

[98] S. Wußow, L. Sitzki and T. Hahm. 3D-simulation of the turbulent wake behind a wind turbine. *Journal of Physics Conference Series*, 75: 12036–12036, 2007.

[99] A. Zervos, S. Huberson and A.Hemon. Three-dimensional free wake calculation of wind turbine wakes. *J. Wind Engng and Industrial Aerodynamics*, 27:65–76, 1988.